frontiers in Materials

REVIEW
published: 10 January 2022
doi: 10.3389/fmats.2021.816309

A Focused Review on Engineering Application of Multi-Principal Element Alloy

Yang Chen[1†], Baobin Xie[1†], Bin Liu[2], Yuankui Cao[2], Jia Li[1], Qihong Fang[1]* and Peter K. Liaw[3]**

[1]State Key Laboratory of Advanced Design and Manufacturing for Vehicle Body, Hunan University, Changsha, China, [2]State Key Laboratory of Powder Metallurgy, Central South University, Changsha, China, [3]Department of Materials Science and Engineering, The University of Tennessee, Knoxville, TN, United States

Compared with traditional alloys with one principal component up to 40–90%, multi-principal element alloys (MPEAs) were born in the complicated intermingling of traditional and non-traditional physical metallurgy, and brings us a great amount of excellent performances. Here, we would briefly summarize the potential applications in some key areas, which is helpful for latecomers to quickly and comprehensively understand this new alloy system. Especially, the applications of MPEAs in aerospace, industrial equipment, national defense, energy, navigation and so on are discussed roughly. Subsequently, several emerging areas have also been compared. Finally, some suggestions are given for the future development trend.

Keywords: multi-principal element alloys, engineering applications, mechanical properties, chemical properties, physical properties, biology

OPEN ACCESS

Edited by:
Zhenyu Li,
University of Science and Technology of China, China

Reviewed by:
Fuyang Tian,
University of Science and Technology Beijing, China
Yong Ni,
University of Science and Technology of China, China

****Correspondence:***
Jia Li
lijia123@hnu.edu.cn
Qihong Fang
fangqh1327@hnu.edu.cn
Peter K. Liaw
pliaw@utk.edu

†These authors have contributed equally to this work

Specialty section:
This article was submitted to Computational Materials Science, a section of the journal Frontiers in Materials

Received: *16 November 2021*
Accepted: *21 December 2021*
Published: *10 January 2022*

Citation:
Chen Y, Xie B, Liu B, Cao Y, Li J, Fang Q and Liaw PK (2022) A Focused Review on Engineering Application of Multi-Principal Element Alloy. Front. Mater. 8:816309. doi: 10.3389/fmats.2021.816309

INTRODUCTION

Metallic materials play an irreplaceable role in the development of industrial civilization, from Bronze Age (about 3000 BC) to intelligent age (since the 21st century). Conventional alloys, such as copper-based alloys, aluminium-based alloys, magnesium-based alloys, and iron-based stainless steel are usually composed of one or two major elements, introducing other metallic/non-metallic elements with appropriate ratios into them to obtain desired performance (Esmaily et al., 2017; Lee et al., 2018; Li et al., 2018; Sun B. et al., 2021). Obviously, this traditional alloy design concept has not satisfied the growth demand about special function materials in modern industrial civilization due to huge limitation on the composition space.

In the past two decades, multi-principal element alloys (MPEAs) or high entropy alloys (HEAs, consisting of five or more elements) with equal or near-equal mole ratio have attracted widespread attention from related researchers because of their excellent properties in mechanics, chemistry and biology (Yeh et al., 2004; Zhang et al., 2014; Li et al., 2016; Yao et al., 2018; Xie et al., 2019). This trend can be attributed to their unique four core effects, i.e., high-entropy effect, sluggish diffusion, cocktail effect, and lattice-distortion effect. High configuration entropy can effectively prevent the formation of harmful intermetallic compounds like some brittle phases because it significantly reduces the Gibbs free energy of a system, thus promoting the formation of single-phase solid solutions, such as face-centered-cubic (FCC) structure, body-centered-cubic (BCC) structure, and hexagonal-close-packed (HCP) structure in MPEAs (Miracle and Senkov, 2017). A sluggish diffusion effect contributes to hinder grain growth, boost the nucleation of nanoprecipitation, and increase the recrystallization temperature, which is conducive to further tuning microstructures of MPEAs, thus

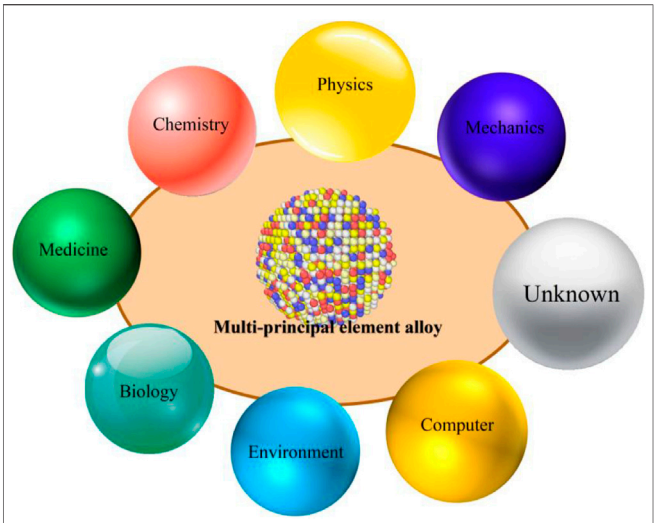

FIGURE 1 | Potential engineering applications of MPEAs.

enhancing the comprehensive properties (Tsai et al., 2013). Severe lattice distortion induced by different atom sizes can improve the lattice-fraction stress and become a strong impediment to the dislocation movement, resulting in significant solution strengthening in MPEAs (Tsai et al., 2013). The complexity and variety of MPEAs might be attributed to the cocktail effects. The addition of a lightweight alloying element reduces the density of MPEAs, and furthermore, the introduction of refractory alloying elements significantly improves the melting points of MPEAs. Moreover, the complex interactions between each alloying element further impact the performance of MPEAs (Ranganathan, 2003). For instance, the effect of the Al element in Al_xCoCrCuFeNi MPEAs is investigated (He et al., 2014). The results suggest that increasing the Al element can enhance the strength whereas decreasing the ductility. This is because that the addition of the Al element promotes the formation of the BCC phase, which acts as a hardening phase.

Up to now, MPEAs as advanced engineering materials have been widely investigated in various fields. For example, four-point-bending high-cycle fatigue and fatigue-crack-growth behaviors of MPEAs are summarized, indicating that before the crack occurs, the plastic deformation behavior is dominated by the nanotwinning (Chen et al., 2018). The effects of composition, crystal structure, valence electron concentration, mixing entropy on the superconducting transition temperatures are reviewed, suggesting that MPEAs can be regarded as a promising superconducting material (Sun and Cava, 2019). In addition, the corrosion-resistant performance of MPEAs and their coatings in various kinds of aqueous solution are discussed in detail. Meanwhile, the influence of composition and processing method on the corrosion resistance are summarized. The results show that element homogenization can significantly improve the corrosion resistance of MPEAs (Shi et al., 2017). However, there is still a lack of a systematic review about engineering/industrial applications of MPEAs. In this review, we will collect and sort out the potential applications in related fields, to navigate the reasonable research direction in the future.

CLASSIFICATION OF ENGINEERING APPLICATION

To clearly describe the potential applications of MPEAs, the following aspects are divided based on their performances, as shown in **Figure 1**. For example, the required characteristics of automotive engine materials are high strength for resistance to the combustion pressure, good ductility for preparation of complex engine structures, and light for low carbon energy saving. Here, "7 + X" application areas are discussed in the following section.

MECHANICS

The characteristics of engineering materials under various forms of loads are called mechanical properties. Metal materials must reach certain mechanical properties to meet the engineering needs.

Strength and Toughness

Metal materials will deform and even cause damage under the action of an external force. The strength of materials refers to the ability of metal materials that resists plastic deformation and fracture under the action of force. Machine parts often bear impact loads during service process. At this time, toughness is used to measure the performance of materials. Toughness refers to the deformation energy absorbed by metal materials before fracture. The FCC MPEA has good plasticity (Gludovatz et al., 2014), which is a good matrix material. The BCC MPEA has high strength and low toughness, compared with the FCC MPEA (Zou et al., 2014; Senkov and Semiatin, 2015; Gao et al., 2016; Li et al., 2020c; Feng et al., 2020; Peng et al., 2021). Different from the microstructures of traditional alloys, it induces special deformation mechanisms and leads to excellent strength and toughness.

The equiatomic FeCoCrNiMn MPEA with an FCC single solid-solution phase prepared by a rolling-recrystallization process has excellent damage tolerance at low temperatures (Gludovatz et al., 2014), owing to the multiple deforming machine to improve toughness. At the initial stage of deformation, the significant lattice friction of the MPEA makes it difficult for dislocations to move and increases the strength. In the later stage of deformation, due to the low stacking fault energy of FeCoCrNiMn, deformation twins are generated at the crack tip to prevent crack propagation. This toughness level can be compared with several of the best low-temperature steels, such as some austenitic stainless steels and high nickel steels.

By adjusting the alloy composition, such as reducing the content of Co and Ni and Mn, to reduce the room temperature and low-temperature stability of the FCC phase,

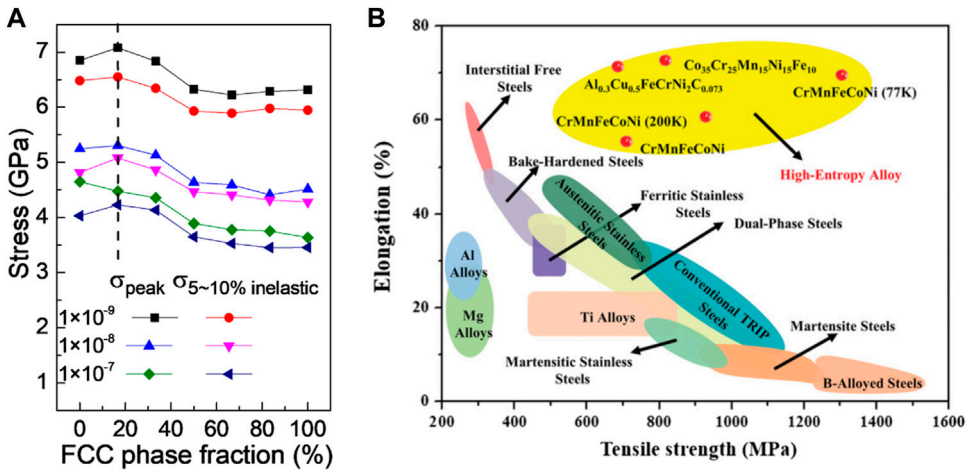

FIGURE 2 | (A) Yielding stress vs. FCC phase fraction at different strain rates (Fang et al., 2019). **(B)** The strength and toughness between MPEAs and other conventional alloys (Liu et al., 2021).

the deformation-induced transformation-strengthening can occurs in the MPEA, resulting in very considerable strengthening and plasticizing effect (Bae et al., 2018; Fang et al., 2019; Li et al., 2016; Ren et al., 2021) (**Figure 2A**). Transformation induced plasticity (TRIP) includes FCC→HCP and FCC→BCC. The deformation induced FCC→HCP transformation process of the $Cr_{20}Mn_6Fe_{34}Co_{34}Ni_6$ MPEA leads that its room-temperature tensile strength reaches 1 GPa and tensile plasticity approaches 60% (Fang et al., 2019; Chen et al., 2020). Through the deformation induced FCC→BCC transformation strengthening mechanism, the tensile strength of the $V_{10}Cr_{10}Co_{30}Fe_{50}$ dual phase MPEA at 77 K increases to 2 GPa (Kim et al., 2019).

A variety of principal components of MPEA leads to a strong atomic-radius mismatch and modulus mismatch between different elements to provide a good solid-solution-strengthening effect, which has a typical application in the room-temperature and high-temperature strengthening of the refractory high entropy alloy (RHEA) of the BCC phase (Senkov et al., 2011a; Senkov et al., 2011b). NbMoTaWV with high strength and low toughness and HfNbTaTiZr with high toughness and low strength are two classical BCC RHEA systems. Thus, the addition of W and Mo elements with high melting points into HfNbTaTiZr causes additional solid solution strengthening to improve room temperature strength, and maintains toughness (yield strength reaches 700 MPa, and fracture strain approaches 35% at 1,200°C) (Wang M. et al., 2019). The oxygen-containing ordered oxygen complexes (OOCs) formed in HfNbTiZr by doping O atoms (Lei et al., 2018). The pinning effect of OOCs on dislocations is stronger than that of interstitial atoms to promote dislocation cross slip, which leads to a large number of dislocation proliferation and induces high strength and toughness (Lei et al., 2018). On the whole, MPEAs have excellent strength and toughness compared with other conventional alloys (**Figure 2B**).

Wear Resistance

With the rapid development of aerospace, marine and automotive industries, the friction and wear of power systems and moving parts are more serious. Harsh working conditions put forward higher requirements for the wear resistance of friction pair materials. The wear failure of materials has become a technical bottleneck restricting the rapid development of this field. However, the use of existing conventional materials has reached their limit. MPEAs have excellent wear resistance due to the special effects different from traditional alloys, such as lattice distortion and high entropy effect (Yeh et al., 2004). Many MPEAs have better wear resistance than conventional wear-resistant alloys including SKD61 steel and SUJ2 steel (**Figure 3A**). MPEA wear-resistant materials mainly include MPEA bulks and MPEA coatings.

The near-infinite compositional space and solid-solution structures of MPEAs provide a huge configuration space for designing new wear-resistance materials (Ding et al., 2019). Many studies have shown that phase structure improves the wear resistance. By arc-melting and casting, the body-centered-cubic (BCC) matrix and L_{21} phase make the $Al_{0.25}Ti_{0.75}CoCrFeNi$ MPEA the promising candidate for mechanical wear-resistant applications (Gwalani et al., 2018). In MPEAs, the appearance of sigma-phase precipitation in some annealing process hinders the dislocation movement, improving the hardness and leading to excellent wear resistance. By sliding wear at intermediate temperatures (600–800°C), sigma-phase precipitation occurs in the recrystallized wear subsurface of CoCrFeMnNi MPEA, which causes the excellent wear resistance (Joseph et al., 2020). By the annealing process, the sigma phase precipitates occur in the $AlCoCrFeNiTi_{0.5}$ MPEA, causing the better wear resistance of $AlCoCrFeNiTi_{0.5}$ MPEA than the conventional alloys of 1Cr18Ni9Ti stainless steel, SiC ceramic preserves, and ZrO_2 ceramic (Yu et al., 2014).

In fact, the proportion and type of composition elements determine the solid-solution structure related wear resistance.

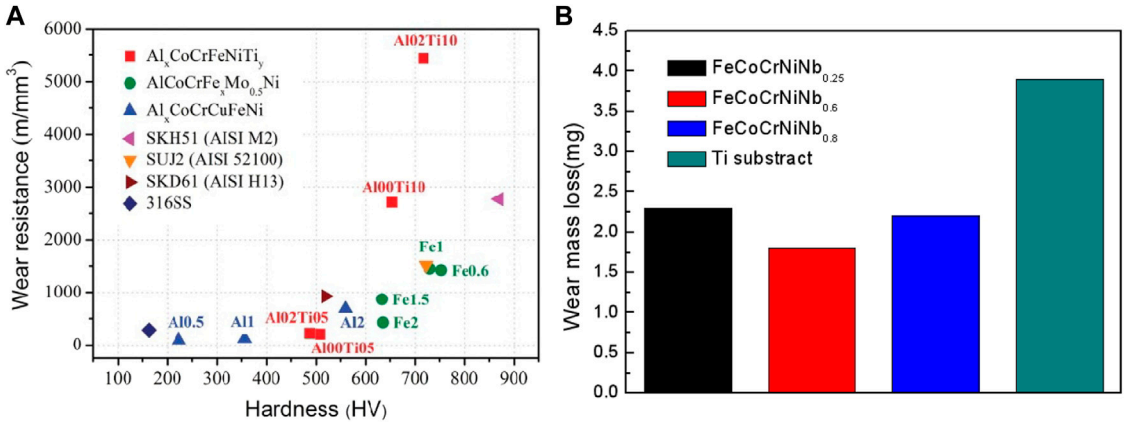

FIGURE 3 | (A) The hardness vs. wear resistances of various HEAs and other conventional alloys (Wu et al., 2006; Hsu et al., 2010; Chuang et al., 2011; Tsai and Yeh, 2014). **(B)** Wear resistance of FeCoCrNiNbx MPEA coatings (Fang et al., 2018).

The additions of Al, V, and Ti elements in MPEAs induce the formation of a strong BCC phase in the matrix, increasing the hardness to improve the wear resistance of MPEAs (Tong et al., 2005; Chen et al., 2006; Löbel et al., 2018). In $Al_xCoCrCuFeNi$ MPEAs, the AlCoCrCuFeNi MPEA has better wear resistance, which is mainly attributed to the increased strong bcc phase caused by Al element (Tong et al., 2005). The TiZrHfNb RHEA is prepared by arc melting, based on refractory elements (Ti, Zr, Hf, and Nb), which exhibits the improved wear resistance in comparison with the traditional superalloy of the pure Nb, C103 (Nb-5.4Hf-2Ti), and a commercial superalloy (Inconel 718), resulting from a higher hardness/strength induced by a strong BCC solid solution (Poulia et al., 2016; Ye et al., 2018). The Pb and B elements combine with other elements in MPEAs to produce precipitation, which hinders the movement of dislocations, increasing hardness to improve wear resistance (Liu et al., 2016; Yadav et al., 2018). With the addition of boron in the $Al_{0.5}CoCrCuFeNiBx$ MPEA, boron element forms borides instead of entering the crystal structure to significantly improve wear-resistance, owing to the combination of the large hard borides and ductile and tough FCC matrix (Liu et al., 2016).

The application range of MPEA bulk materials is limited due to the preparation process, materials and preparation cost. When MPEAs are used as coating materials, their flexible preparation process, controllable preparation cost, and excellent performance are suitable for extreme environments in the modern industry. A laser cladding (LC) technology is a process of melting and rapid solidification of metal powder by high-energy laser beam, which is widely used to prepare MPEA coatings. Therefore, the compositions of MPEAs has a great influence on the wear resistance. The Al and Ti elements can promote the formation of a strong BCC phase to improve wear resistance (Cui et al., 2020; Jin G. et al., 2018; Liu et al., 2020; Qiu et al., 2014). For the $FeCoCrNiMnAl_x$ MPEA coatings, weight loss of the $FeCoCrNiMnAl_{0.75}$ cladding layer is approximately 58 and 17% of those of the base metal, respectively (Cui et al., 2020). In the $Al_2CrFeNiCoCuTix$ MPEA coatings, the wear resistance of $Al_2CrFeNiCoCuTi_{0.5}$ MPEA coating is better due to the coexistence of BCC and FCC phases (Qiu et al., 2014). The addition of the Nb element changes the phase structure of the coating, which affects the wear resistance of the coating, as shown in **Figure 3B** (Fang et al., 2018; Liang et al., 2019). The microhardness of $AlCrFeNi_2W_{0.2}Nb_x$ coatings increases with the increasing Nb content, and the wear resistance of $Nb_{1.5}$ is excellent (Liang et al., 2019). Boronizing and nitriding are a thermochemical surface-hardening process that improves the surface mechanical performances by the formation of borides and nitrides generated in the diffusion of B and N atoms into the surface of metals/alloys at high temperatures (Wang et al., 2018; Hou et al., 2019). The wear quality with unboronized condition is 12 times of that in the boronized $Al_{0.25}CoCrFeNi$ MPEAs (Hou et al., 2019). The hardness of the nitrided AlCoCrFeNi MPEA increases from HV 522 HV of the as-cast AlCoCrFeNi MPEA to 720 HV of the nitrided MPEA (Wang et al., 2018).

Creep Resistance

The phenomenon of slow inelastic deformation of metal materials under certain temperature and stress is called creep. Because different forms of fracture failure can occur in metal materials during creep, it is of great significance to study the creep behavior. The MPEA has extraordinary mechanical properties, including the excellent creep resistance, which plays an important role in engineering application at room temperature and low stress, owing to strong diffusion resistance caused by the lattice distortion arising from the difference in atomic sizes (Kang et al., 2018; Tsai et al., 2018; Zhang M. et al., 2021). The CrMnFeCoNi MPEA exhibits excellent creep resistance compared to nickel base alloys as shown in **Figure 4** (Gadelmeier et al., 2020). The high creep resistance of CoCrFeMnNi at intermediate temperatures (0.2–0.6 Tm where Tm is the melting temperature) is attributed to the solution strengthening from the large atomic-size misfit of Cr (Kang et al., 2018). The nanosized oxides formed in the MPEA matrix via selective laser melting and mechanical alloying suppress the dislocation movement, which invokes a threshold to improve the high-temperature creep resistance of MPEA (Hadraba et al., 2017; Dobeš et al., 2018). It suggests a way for

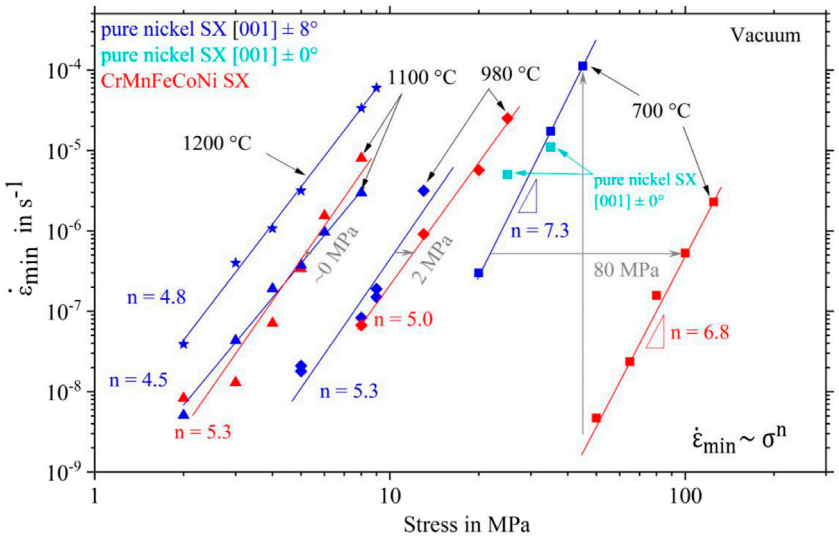

FIGURE 4 | The log-log of minimum creep rate vs. stress of the CrMnFeCoNi MPEA compared with pure nickel at different temperature (Gadelmeier et al., 2020).

improving the high-temperature creep resistance of MPEAs using in-situ-formed oxide via high oxygen content in pre-alloy powders.

The compositions of MPEAs can be tuned to obtain the desired microstructure, including the phase structure, which is also one of the key microstructures affecting the creep properties of MPEAs (Choudhuri et al., 2015; Ma et al., 2016; Kral et al., 2020). Al is added to CoCrFeNiCu MPEA with an FCC structure to prepare a BCC-structured $CoCrFeNiCuAl_{2.5}$ MPEA with a stronger creep resistance via the magnetron sputtering technique (Ma et al., 2016). During creep of the $AlTiVNbZr_{0.25}$ MPEA at 1,073 K and a stress of 100–560 MPa, the formation of Nb2Al-type sigma-phase precipitates at the Zr5Al3/B2 interface hindering the dislocation movement to enhance creep resistance (Kral et al., 2020). The addition of Al not only changes the phase structure, but also improves the dislocation activation volume of MPEA. Compared with traditional alloy, such as Mg alloys, Al alloys, and Ti alloys, $Ti_{30}Al_{25}Zr_{25}Nb_{20}$ MPEA possesses a low creep-strain-rate-sensitive index caused by a high dislocation activation volume, indicating excellent creep properties (Wang D. et al., 2021).

Fatigue Resistance

When subjected to alternating load, many metal materials show the ability to absorb a large amount of accumulated strains before the final failure (Suresh, 1998). The accumulation of fatigue damage leads to crack and final failure, which is a common problem in material applications. For the engineering application of the MPEAs, fatigue fracture is an unavoidable problem (Huang et al., 2007; Miracle and Senkov, 2017). Fatigue-resistant materials of MPEA mainly include MPEA bulks and MPEA films. The single-phase CrMnFeCoNi MPEA has been widely studied, followed by Al-containing CoCrFeNi MPEA and Cu-containing FeMnCoCrSi MPEA.

The microstructure of the material determines the fatigue resistance of the alloy. Due to the ultrafine-grained microstructure delays crack initiation whereas the localized transformation within the crack plastic zone delayed crack propagation, the ultrafine-grained microstructure combined with the transformation-induced plasticity is an effective way to design the next generation of fatigue-resistant alloys (Liu et al., 2018, 2019b; Tian et al., 2019; Picak et al., 2021). The grain-refined $Fe_{42}Mn_{28}Cr_{15}Co_{10}Si_5$ MPEA prepared by friction stir processing exhibits significantly high fatigue strength, as compared with phase transformation induced plasticity steels (Liu et al., 2018). The ultrafine-grained CoCrFeMnNi MPEA prepared by equal channel angular pressing demonstrates a superior fatigue life at relatively low strain amplitude (Picak et al., 2021). The small twin spacing and high twin density would exhibit a remarkable fatigue resistance because of the energy dissipation resulting from detwinning during fatigue loading (Chen et al., 2010; Liu et al., 2014; Hou et al., 2019; Wang et al., 2020). Using radio frequency magnetron sputtering, the CoCrFeMnNi MPEA films with twin spacing spanning across 2 nm show excellent fatigue resistance (Wang et al., 2020). Nanotwinned nanocrystalline CoCrFeNi MPEA film prepared by magnetron sputtering shows the high stability of twin boundaries during cyclic tests because the extremely-stable correlated necklace dislocations moved back and forth along the twin boundaries (Huo et al., 2019).

Compared with other conventional alloys, MPEAs show strong application potentials about great fatigue resistance, due to the abundant compositional space available for MPEAs. **Figure 5** compares fatigue limit and fatigue ratio in a set of structural materials (Abareshi and Emadoddin, 2011; Fredj et al., 2004; Haidemenopoulos et al., 2013; Hemphill et al., 2012; Islam et al., 2007; Koyama et al., 2017; Ly and Findley, 2016; Sugimouto et al., 1997). The fatigue ratio is defined as the ratio of the fatigue-endurance limit to the ultimate tensile strength (UTS), to further

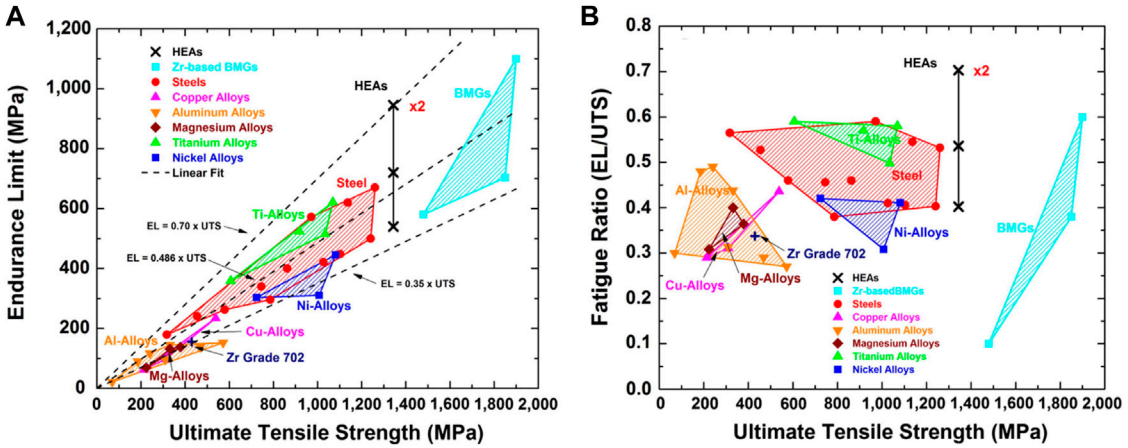

FIGURE 5 | (A) the endurance limit and **(B)** fatigue ratio vs. UTS for Al0.5CoCrCuFeNi MPEA and other structural materials (Hemphill et al., 2012).

compare the fatigue properties between MPEAs and other alloys (Tang et al., 2015). The DP-5Si HEA has a high fatigue strength than all TRIP steels (Liu et al., 2018), thereby indicating its strong engineering application in cyclic loading. This result is attributed to that both the fatigue limit and UTS can be simultaneously improved by the TRIP effect caused by a metastable γ phase and ultrafine-grained microstructure with the addition of Si. The relationship between the fatigue ratio and UTS shows that $Al_{0.5}$CoCrCuFeNi MPEAs have relatively high-endurance limits attributed to a two-phase structure with the addition of the Al element (Tang et al., 2015). The lower points of the fatigue ratios of the MPEAs are at the same level, compared with those of steels, Ti alloys, Ni alloys, and Mg-alloys, However, the upper bound is greatly higher than other alloys in the figure (Tang et al., 2015). Overall, **Figure 5** suggests that MPEAs have great fatigue strengths for engineering applications (Hemphill et al., 2012).

Suggested Future Investigation

In summary, the type and content of the constituent elements of MPEA, the phase structure, the preparation process and the grain size play a key role in the mechanical properties (including strength, wear resistance, creep and fatigue), and have been extensively studied. In addition, there are some new research directions to improve their mechanical properties, such as eutectic structure and gradient structure (Jin X. et al., 2018; Chen et al., 2019; Feng et al., 2021; Joseph et al., 2018).

PHYSICS

In addition to excellent mechanical properties, MPEAs also have attractive physical properties, such as magnetism, resistance, superconductivity and so on (Ye et al., 2016).

Magnetic Behavior

The magnetic properties of alloys are sensitive for component. For MPEAs containing multiple principal element, the addition of more ferromagnetic elements makes it easier to have excellent

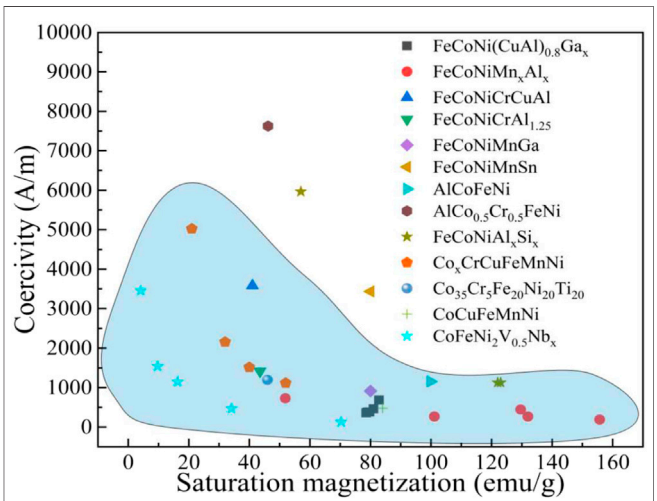

FIGURE 6 | Saturation magnetization vs. coercivity for different MPEA (Li et al., 2021a).

magnetic properties. There are many studies on the magnetic properties of MPEAs obtained by adding two elements with an equal molar ratio to the FeCoNi matrix, including FeCoNi(A1Si)x (Zhang et al., 2013), FeCoNi(MnSi)x (Li et al., 2019), FeCoNi(NiAl)x (Zhang X. K. et al., 2021), FeCoNi(CuAl)x (Zhang Q. et al., 2017), and FeCoNi (MnAl)x (Li et al., 2017a). The FeCoNi(A1Si)x MPEA with x = 2 presents typical soft magnetic characteristics, which has the characteristics of high saturation magnetization (Ms) and low coercivity (Hc) (Zhang et al., 2013). Here, Ms is the maximum magnetization that can be excited in the external magnetic field; Hc is a physical quantity reflecting the difficulty of the ferromagnet in the excitation and demagnetization stages. Higher Ms/Hc shows better soft magnetic property. The $CoFeMn_{1.2}NiGa_{0.8}$ exhibits better soft magnetic properties than most reported MPEAs (Sun X. et al., 2021), indicating the addition of Ga can improve the magnetic properties.

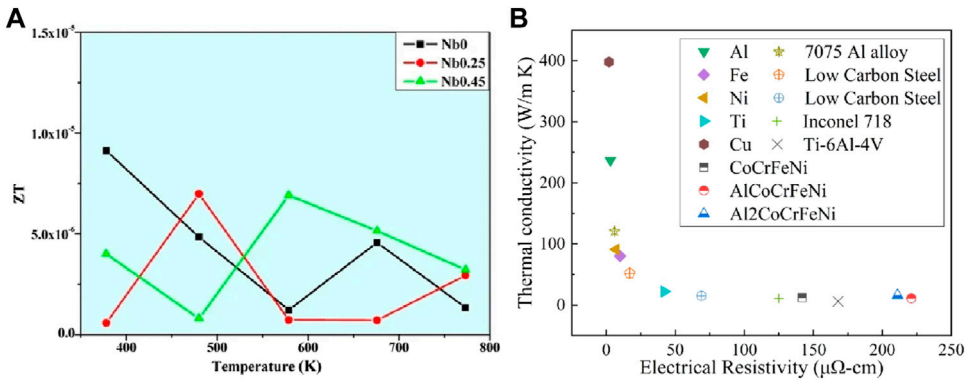

FIGURE 7 | (A) Thermoelectric figure of merit vs. temperature for CoCrFeNiNbx MPEA (Han et al., 2020). **(B)** The relationship between electrical resistivity and thermal conductivity for MPEAs and conventional alloys (Chou et al., 2009; Kao et al., 2011).

The phase constitutions changed by alloying or phase transformation play an important role on the magnetic properties of MPEAs (Marshal et al., 2019; Zhao C. et al., 2021). With the addition of Al in the FeMnCoCr MPEA, the formation of the BCC structure shows a ferromagnetic behavior (Marshal et al., 2019). In the AlCoCrFeNi MPEA, the BCC phase plays a major role to provide a high Ms, but the FCC phase has no effect on magnetic properties (Zhao D. Q. et al., 2021). The effect of the processing technology on the magnetic properties can not be ignored. The annealed $FeCoNiMn_{0.25}Al_{0.25}$ MPEA exhibits the high Ms and low Hc (Li et al., 2017b), and shows better soft magnetic properties than most other commercialized soft magnets. Therefore, MPEAs have great development potential in the fields of the large power grid equipment, and high-frequency magnetic communication due to excellent magnetic properties (**Figure 6**).

Electrical Property

At present, MPEAs have potential applications in the thermoelectric (TE), conductive, and resistive materials due to their good electrical properties. In the global energy shortage environment, the TE generator with efficient waste heat recovery will be an important means to supplement energy in the future. Compared with the traditional TE materials suitable for the low-temperature region, MPEAs are a potential high-temperature TE material (Fan et al., 2017; Han et al., 2020; Shafeie et al., 2015), due to their rich elemental compositions. The La addition improves the Seebeck coefficient and conductivity of the PbSnTeSe MPEA at high temperatures (Fan et al., 2017). As shown in **Figure 7A**, an appropriate amount of Nb was added to CoCrFeNi to obtain a bulk $CoCrFeNiNb_{0.45}$ eutectic high-entropy alloy (EHEA) with excellent thermal stability. CoCrFeNiNb0.45 EHEA has a higher thermoelectric figure of merit (ZT) at high temperatures (T > 573 K), showing a great prospect of thermoelectric applications at elevated temperatures (Han et al., 2020). The reduction of the lattice thermal conductivity is one of the most effective ways to improve the properties of thermoelectric materials. In the $Sn_{0.25}Pb_{0.25}Mn_{0.25}Ge_{0.25}Te$ MPEA with excellent thermoelectric properties, the configurational entropy increases to enhance the phonon scattering because various elements exist at the cationic (Sn2+) site, leading to a reduced lattice thermal conductivity (Wang X. et al., 2021). Thus, the high entropy alloying is an effective strategy to reduce the lattice thermal conductivity for improving the thermoelectric property.

For achieving higher integration and reliability, the rapid technological progress of nanoscale manufacturing equipment requires the development of advanced resistance films. Lattice distortion can greatly increase the resistivity of the material. The nanotwinned nanocrystalline CoCrFeNi MPEA film prepared by magnetron sputtering has a resistivity as high as 135.1 μΩ cm. The high resistivity is attributed to the strong blocking effect caused by lattice distortion (Huo et al., 2018). The NbMoTaW MPEA films have a strong size-independent electrical resistance (~170 μΩ cm) (Feng et al., 2018). Hence, lattice distortion plays a major role in resistance. In some industrial applications, the electrical conductivity of the film is also very important. For example, the protective film of the electrical contact plug should have a low resistivity. The Cu addition improves the conductivity of HEAs (Huang K. et al., 2021). The increase of the Cu content changes the electronic structure of the $AlCuxNiTiZr_{0.75}$ MPEA film, causing the resistivity to drop sharply to 66 μΩ cm at x = 1.4 (Huang K. et al., 2021). The electrical resistivity of MPEAs (from 100 to 220 μω·cm) is 1-2 orders of magnitude than that of many conventional metals, and is similar to that of some bulk metallic glasses (BMGs) (**Figure 7B**).

Thermal Property

According to the formula $K(T) = \alpha(T) \times S(T) \times \rho(T)$, thermal conductivity K(T) is generally obtained by measuring the thermal-diffusion coefficient, $\alpha(T)$, specific heat, S(T), and density, ρ(T), of the material at a temperature T, which is an indicator used to measure the thermal-conductivity capacity of materials. The effect of the Al addition on the thermal conductivity is studied in $FeCoCrNiNb_x$, $Al_xCoCrFeNi$ and $Al_xCrFe_{1.5}MnNi_{0.5}Moy$ alloys (Chou et al., 2009; Lu et al., 2013). Thermal conductivity of $Al_xCoCrFeNi$ alloys is from 10 to 27 W/m·K, and lower compared to that of most pure metals. It

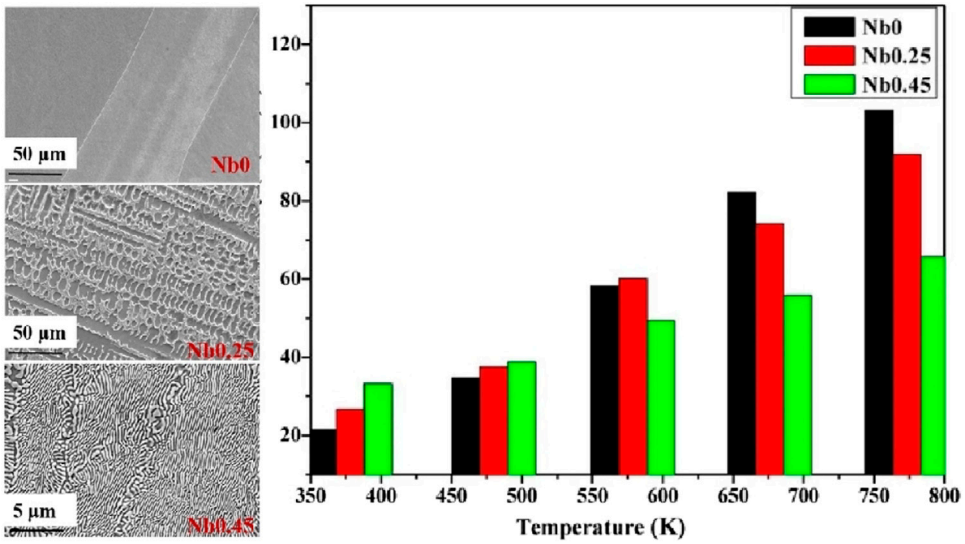

FIGURE 8 | The microstructure and thermal-conductivity of FeCoCrNiNbx MPEA (Han et al., 2020).

is equal to that of heavily-alloyed metals, such as the high-alloy steel and Ni-based alloy (Chou et al., 2009; Shackelford and Alexander, 2000). As shown in **Figure 8**, the low thermal-conductivity of $CoCrFeNiNb_{0.45}$ MPEA is attributed to the full eutectic microstructure (Han et al., 2020). The low thermal conductivity of MPEAs is credited to lattice distortion, which causes the serious scattering of phonon. Under medium temperature conditions (from 27°C to 300°C), the thermal conductivity of Al added MPEAs raises with the addition of temperature (Chou et al., 2009; Lu et al., 2013) attributed to the addition of mean-free path of phonon, and the lattice thermal expansion caused by high temperature (Lu et al., 2013). The stainless steel and Inconel alloy have the same trend as Al added MPEAs, but most pure alloys are opposite (Shackelford and Alexander, 2000; Chou et al., 2009). For the $Al_xCoCrFeNi$ MPEA, the thermal conductivity in a duplex single-phase region is lower than that in the single phase region, owing to the additional scattering from FCC/BCC phase boundaries (Chou et al., 2009). In the $Al_xCoCrFeNi$ MPEA, the electrical conductivity reduces with the increase of temperature. The electrical conductivity shows an opposite trend compared to the thermal conductivity with the increase of temperature. Thus, the Wiedemann-Franz law does not apply for the $Al_xCoCrFeNi$ MPEA (Chou et al., 2009). The relationship between thermal expansion coefficients (TEC) and Al content has been studied in the $Al_xCoCrFeNi$ alloys (Chou et al., 2009). The TEC of the $Al_xCoCrFeNi$ MPEA reduces with the addition of Al content, owing to the formation of the BCC phase. Thus, the BCC phase structure has the effect of reducing TEC in MPEAs.

Optical Property

With the rapid development of society, energy problems have become increasingly acute. The use of solar energy to obtain thermal energy is an energy harvesting technology that effectively utilizes renewable energy, which can effectively alleviate the increasing energy contradiction (Selvakumar and Barshilia, 2012). Solar selective absorbing coatings (SSACs) are the key components of the concentrating solar power (CSP) systems, among which the spectral selectivity and thermal stability of SSACs are the most important indicators (Wang X. et al., 2017). In order to improve the efficiency of the light-to-heat conversion, SSAC should have high solar absorptance (α) and low thermal emittance (ε) (Gao et al., 2017). Transition metal nitrides have excellent electrical and optical properties (Wu et al., 2015). The high-entropy alloy nitrides (HEANs) synthesized with refractory elements have become an ideal material for manufacturing SSAC, due to their excellent high-temperature resistance and optical properties. The optical properties of NbMoTaWN, MoNbHfZrTiN, and MoTaTiCrN HEANs are investigated, showing the exceptional spectral selectivity (α/ε = 0.944/0.12, 0.934/0.09, and 0.923/0.065 for NbMoTaWN, MoNbHfZrTiN, and MoTaTiCrN) (Guo et al., 2020; He et al., 2020; Yu D. M. et al., 2021; Yu D.-M. et al., 2021; He et al., 2021). These HEANs show excellent thermal stability and corrosion resistance. After annealing at 600°C for 100 h, NbMoTaWN still maintains good optical properties (α/ε = 0.902/0.106) (Yu D.-M. et al., 2021). For MoNbHfZrTiN, the solar absorptance and thermal emittance are only slightly raised and lowered, respectively, (α/ε ranges from 0.935/0.09 to 0.912/0.11) in a 3.5% NaCl solution for 24 h at room temperature (He et al., 2020). The Al, Si, and Cr elements added in MPEA combine with oxygen to produce an oxide film on the surface at high temperature, which gives a barrier for the prevention of further oxidation to improve oxidation resistance. Therefore, MPEAs containing Al, Si and Cr have excellent high temperature thermal stability. AlCrTaTiZrN MPEA has excellent spectral selectivity (α/ε = 0.928/0.051), high temperature thermal stability (little change in the spectral selectivity after annealing at 800°C for 2 h), and long-time thermal stability (little change in the spectral selectivity after annealing at 650°C for 300 h) (He et al., 2021). In addition,

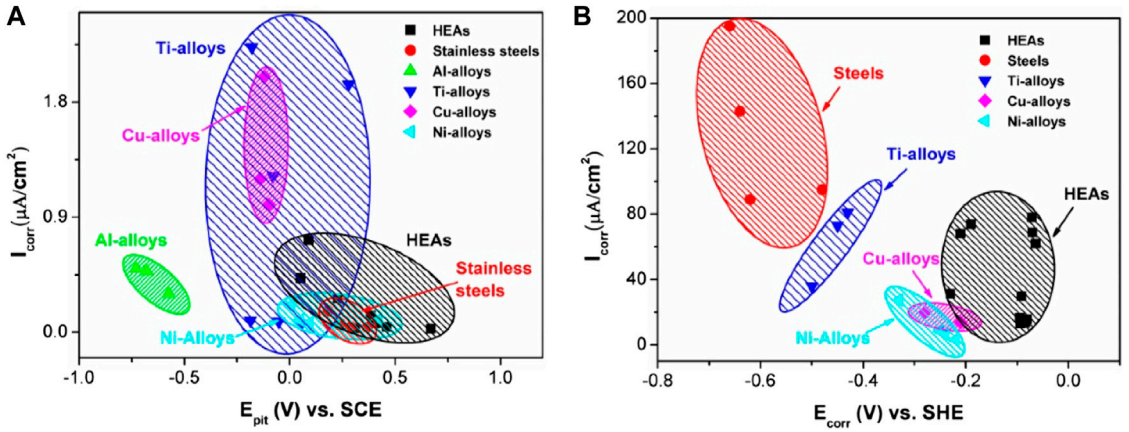

FIGURE 9 | The relationship between the corrosion-current density and pitting/corrosion potentials of MPEAs and conventional alloys, respectively, in a salt solution **(A)** and acid solution **(B)** (Shi et al., 2017).

AlCrTaTiZrN MPEA achieves the optimal photothermal conversion efficiency at high sunlight exposure (He et al., 2021). Thus, MPEAs with excellent optical and thermal stability properties have the great application potential for the solar-thermal technology.

Challenge and Prospect

In short, the magnetic and optical properties of MPEAs are sensitive for element composition and phase structure. The configuration entropy and lattice distortion are the key factors to control the thermal and electrical conduction of MPEA. Furthermore, there are some challenging topics that need to be studied in depth, including the effects of magnetic moments (Tsai, 2013), spin (Niu et al., 2015), hall coefficient (Kao et al., 2011), and lattice vibration (Körmann et al., 2017) on physical properties.

CHEMISTRY

Corrosion Resistance

Corrosion is a chemical/electrochemical reaction process between materials and ambient media, such as water, air, acid, and alkali, which greatly affects the service performance and even causes the failure (Hansson, 2011). From a thermodynamic point of view, most of metals, except for some noble metals like Au, Ag, and Pt, are in an unstable state, and tend to oxidize with the ambient medium to form metal oxides. Hence, metal corrosion occurs (Song and Atrens, 2003). In past decades, the corrosion resistance is usually achieved by introducing alloying elements (Cr, Ni, and Mo) into Ni-based alloys, stainless steels, or Ti-based alloys to form a protective passive film on the metal surface (Gupta and Birbilis, 2015). However, the existence of precipitates during the metallurgical process and poor-high temperature stability significantly worsen their corrosion-resistance and mechanical properties, hence limiting their large-scale application in engineering (Nilsson and Wilson, 1993; Cvijović and Radenković, 2006). Recently, MPEAs have been widely reported because of their outstanding corrosion resistance. The corrosion-resistant property of material is usually dominated by the average corrosion rate which can be written as follow:

$$\text{Corrosion\_rate}\left(\text{mm}/\text{year}\right) = 3.27 \times 10^{-3} \times \frac{i_{corr}}{\rho} \times EW$$

where i_{corr} refers to the corrosion-current density, ρ is the alloy density, and EW presents the equivalent weight. It can be seen from **Figure 9** that compared with traditional alloys, MPEAs have much higher pitting potentials (E_{pit})/corrosion potentials (E_{corr}) and lower corrosion current densities (i_{corr}). It suggests their excellent resistance to pitting/general corrosion and outstanding localized corrosion-resistance performance (Shi et al., 2017).

In fact, same as the conventional alloys, the resistance of MPEAs to corrosion can be attributed to the formation of passive films on the surfaces. The difference is that the passivation elements in MPEAs are easier to distribute uniformly, contributing to the formation of the denser oxide film and effectively reducing the hallow formation (Zhang S. et al., 2016; Xiang et al., 2016). Recently, three Co-Cr-Ni-Al-Ti system MPEAs are prepared by vacuum arc melting to investigate the effect of the passivation elements like Co, Cr, and/or Ni on the corrosion-resistant performance (Huang L. et al., 2021). The results indicate that the increment of the Cr element can promote the formation of a passive film Cr_2O_3 in both salt and acid solutions, which plays a significant role in enhancing the corrosion-resistant ability. Meanwhile, the addition of the Co element is helpful for the stability of the passive film, and decreases the hydrolysis of Cr^{3+}. Furthermore, MPEAs containing a Ti element are also widely studied because the presence of a positive electrode potential in the Ti element contributes to form a dense self-healing oxide passivation film. Meanwhile, TiO and TiO_2 passive films not only have great resistance to the acid solution, but also improve their high-temperature oxidation resistance (Liu et al., 2019). Based on this trend, the corrosion resistance of the $AlCoCrFeNiTi_{0.5}$ MPEA is studied in a H_2O_2 solution. The result shows that

the corrosion rate is extremely slow compared to the AlCoCrFeNiCu MPEA (Yu et al., 2015).

On the other hand, the corrosion-resistant performance of MPEA is significantly influenced by different metallurgical processes. Using a laser-cladding-preparation method, the effect of the laser-scanning speed on the corrosion resistance of an AlCrFeCuCo MPEA is investigated (Qiu et al., 2013). The experimental results suggest that the increment of the laser-scanning speed leads to the resistance of the alloy, which firstly becomes better and then worse. The reason for this trend is that lower scanning speed promotes the cooling rate to make a denser surface, whereas a higher scanning speed leads to a rough surface. Moreover, the corrosion resistance of AlCrFeCuCo in a salt solution is better than that in an acid solution. In addition, MPEA coatings with millimetre-scale thicknesses are prepared by electro-spark deposition. Using electro-spark deposition on an AISI 1045 steel, the AlCoCrFeNi MPEA coating has been successfully synthesized, which has a superior corrosion resistance than that of the alloy prepared by casting (Zhang C. et al., 2016). The excellent property stems come from the uniform composition and microstructure as well as the high enough Cr and Al oxide concentrations on the surface. In general, MPEAs have been a promising corrosion-resistant material, which can be suitable for various extreme service environments.

Catalysis

Catalyst not only significantly reduces the energy consumption of reactions, but also effectively improves the reaction speed, and even changes the basic reaction. Therefore, catalyst materials play an irreplaceable role in engineering applications (Guo et al., 2019). Transition metal elements, such as Fe, Cu, Au, Ag, etc. and their alloys are the most widely used catalyst due to their outstanding hydrogenation and dehydrogenation characteristics as well as excellent oxidation and catalytic reforming performance (Tan, 2014). Taking the oxidation of industrial ammonia as an example, PtPdRh-based materials are still the widely employed catalysts. However, the large-scale applications in engineering have been greatly limited by expensive price, high activation-energy-degradation rate, and poor universality (Bagot et al., 2014).

Over the past few decades, the emergency of MPEA has provided an infinity possibility for broadening catalytic materials due to their huge composition space and outstanding catalytic performance. Recently, the equimolar CePdPtRhRu MPEA nanoparticles (NPs) synthesized by the carbothermal shock method have been successfully used in the oxidation of ammonia (Yao et al., 2018). The conversion efficiency of NH_3 using NPs can be up to 100%, and meanwhile, the selectivity to NO_x can reach 99% under a lower temperature. Furthermore, the CePdPtRhRu multimetallic nanoparticles (MMNPs) are made as a comparison by the wet impregnation method. The selectivity to NO_x using MMNPs just approach about 18.7% at the same temperature. The significant improvement of catalyst performance is attributed to the solid-solution phase of NPs rather than phase-separated catalytic materials. Moreover, the increment of the Ru and Ce concentrations not only significantly enhances the catalytic performance, but also reduces the consumption of the precious Pt element. In addition, some researchers are also committed to reducing the content of noble metals like Pt and Ru in catalytic MPEAs. The FeNiCuCoMo MPEA NPs (**Figure 10**) can enhance the decomposition performance of ammonia with an improvement factor of over 20, which exceeds the Ru catalyst and some conventional Co-Mo catalyst (Xie et al., 2019). More interestingly, the catalytic performance can be controlled by tuning the ratio of Co/Mo, thus providing a feasible avenue to maximize the reaction activity at various conditions. More importantly, MPEAs can be used not only for thermal catalysis mentioned above, but also for the methanol oxidation or hydrogen evolution reaction (HER). The NiCoCuFePd MPEA nanotube arrays (NTAs) synthesized by the electrodeposition method show the superior catalyst performance and more stable for the methanol oxidation than conventional Pd NTAs because of their larger surface area and higher mass activity (Wang et al., 2014). It has been reported that the $Ni_{20}Fe_{20}Mo_{10}Co_{35}Cr_{15}$ MPEA exhibits the better HER electrocatalyst performance than that of some precious metallic catalyst, whose overpotential is just 107 mV in the acid solution (Zhang G. et al., 2018). Overall speaking, MPEAs can be the promising next generation catalytic materials.

Suggested Future Direction

MPEAs have been the promising corrosion-resistant and catalytic materials. For further understanding their corrosion and catalytic behavior to design the novel MPEAs with superior performance, some recommended future work is presented below: 1) understand the fundamental reason of corrosion resistance of MPEAs from atomic scale; 2) realize the collaborative design of corrosion resistance and mechanical properties of MPEAs; 3) it is significant to extend the types of supporting substance for improving the catalytic performance of MPEAs; 4) The gaps between theory and experiments in catalytic application of MPEAs should be filled.

COMPUTER

Multiscale Simulations

Based on experiments, simulations effectively improve the basic understanding of the relationship between deformation and performance, and improve performance by optimizing material compositions and structures (Demetriou et al., 2011; Wu et al., 2014; Li et al., 2018). According to the density functional theory (DFT), molecular dynamics (MD) simulations, phase-field method (PFM), and finite element method (FEM), the necessary underlying material parameter, dislocation behaviour, lattice distortion, and phase transformation are investigated in detail (Zhang H. et al., 2018; Rahul et al., 2018; Wang D. et al., 2019; Fang et al., 2019; Yin and Curtin, 2019; Li et al., 2020a; Li J. L. et al., 2020; Sagar et al., 2021), to obtain a deep understanding of microstructure evolution on the mechanical properties of MPEAs.

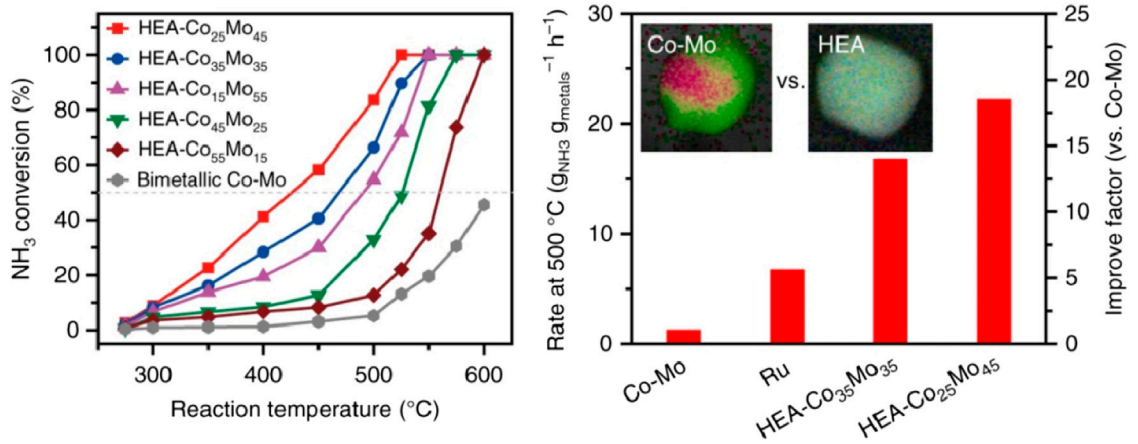

FIGURE 10 | The conversion and rate (T = 500°C) of NH_3 with different Co/Mo ratio (Xie et al., 2019).

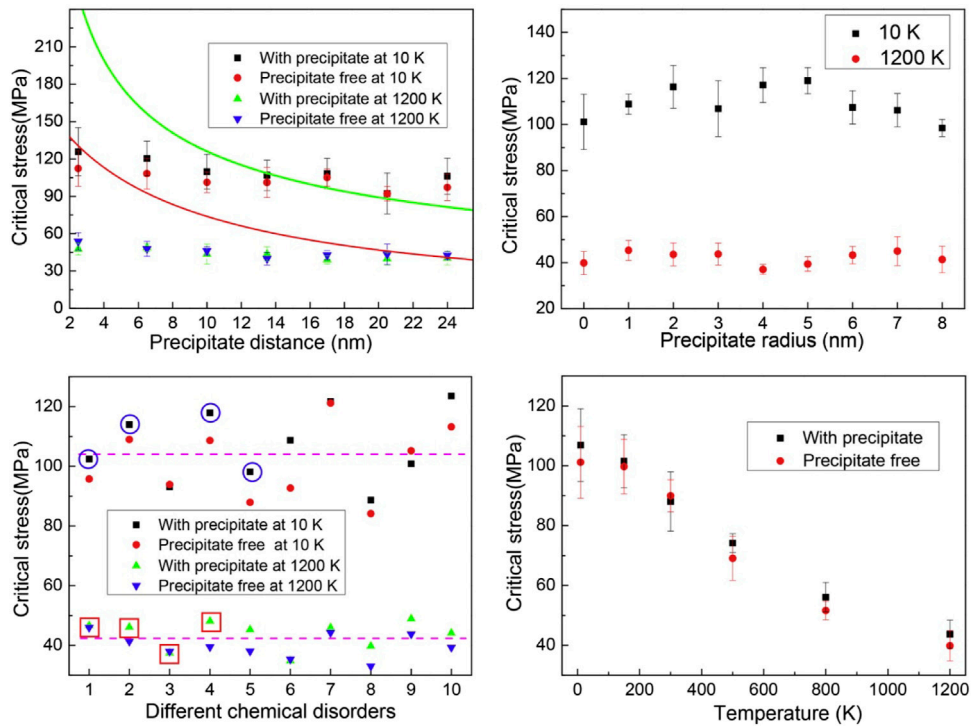

FIGURE 11 | The precipitate spacing, precipitate size, element disorder, and temperature dependence of the critical stress (Li et al., 2020a).

The elemental mismatch volume, lattice/elastic constant, and stable-stacking-fault energy of RhIrPdPtNiCu are calculated by DFT, which are applied in the yield model (Yin and Curtin, 2019). Through MD simulations, the synergistic strengthening of the precipitation and lattice distortion in MPEAs in a wide temperature range is investigated, explaining the effects of temperature, element order, precipitate spacing/size, and dislocation-cut number on precipitates strengthening (Li et al., 2020a) (**Figure 11**). The coherent BCC/B2 microstructure in BCC AlNiCoFeCr MPEA is studied by PFM to reveal the evolution of the microstructure, which is revealed to assist in the design of new MPEAs (Li J. L. et al., 2020). Using FEM, the strain distribution and material flow of the $AlCoCrFeNi_{2.1}$ MPEA give a channel to predict the actual material flow during forging (Rahul et al., 2018). The unique characteristics of MPEAs lead to multi-scale microstructures (atomic-scale lattice distortion, nano-scale short-range order, and micro-scale phase transitions) (Song et al., 2017; Chang

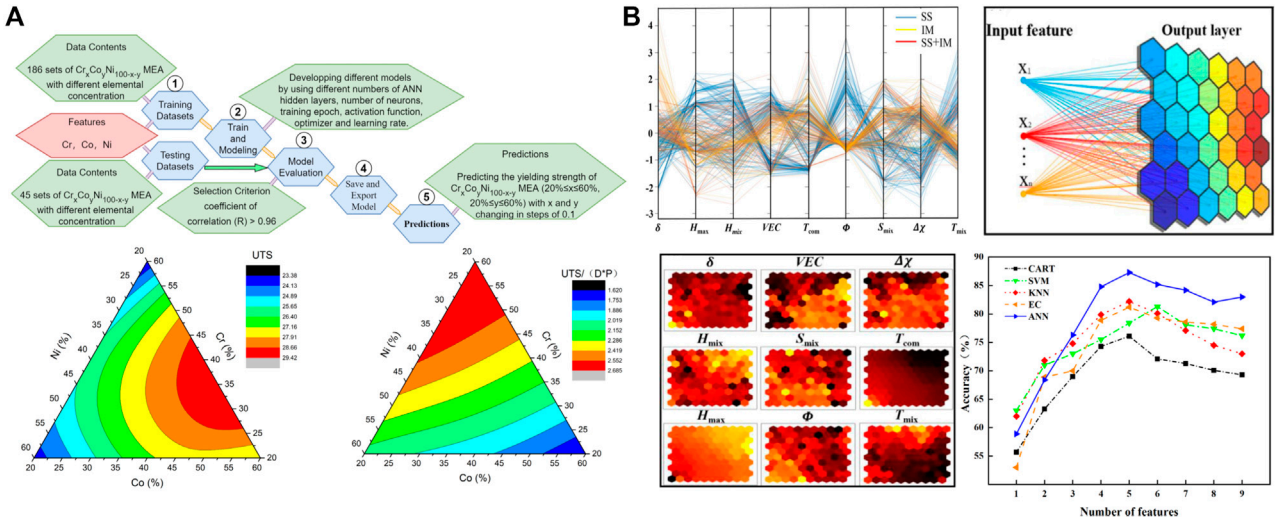

FIGURE 12 | (A) The flowchart of CoCrNi MPEA design strategy by machine learning and high-throughput MD simulations (Li et al., 2021b). **(B)** An artificial neural networks model describing the relationship between elemental characteristics and long-term ordering structure (Zhao D. Q. et al., 2021).

et al., 2020; Seol et al., 2020), however, simulations for traditional alloy are no longer suitable for studying the deformation and strengthening mechanism of MPEAs. Therefore, in order to accelerate the alloy design to further develop new MPEAs for a wide range of industrial applications, it is necessary to use multi-scale simulations to link the microstructure characteristics of MPEAs with their mechanical behaviors.

Machine Learning

The rapid development of the information technology strongly pushes forward the arrival of the "big data" era, when the data acquisition, storage and extraction become easier. The artificial intelligence (AI) driven by mass data has played an irreplaceable role in the modern society. As the powerful tool in AI, machine learning has been widely used in many fields, such as cancer detection, speech recognition and intelligent controls (Zhang et al., 2008; Rupp et al., 2012; Schmidhuber, 2015), because it can look for the best surrogate model to accurately describe the relationship between the data examples without depending on rules-based programming. At present, machine learning has been successfully used in materials science. The combination of a genetic algorithm and artificial neural network is proposed to construct an accurate "composition-heat treatment conditions-mechanical properties" surrogate model of a low alloy steel (Reddy et al., 2015). The high strength and electrical conductivity copper alloys have been successfully designed by the property-oriented machine learning design strategy (Wang C. et al., 2019; Li L. et al., 2021).

The successful application of machine learning on traditional alloy design has prompted to gradually solve MPEA designs. Recent studies have shown that machine learning methods can further improve the mechanical, physical and chemical properties of MPEAs. For example, the feasible material design method integrating machine learning and experiments (Wen et al., 2019) is proposed to look for the MPEAs with higher hardness in the Al-Co-Cr-Cu-Fe-Ni system. Several alloys with superior hardness than the optimum value in the training dataset have been synthesized via seven experiments. Recently, a method combining high-throughput MD simulations and machine learning is proposed to search for the high strength, low cost and density $Co_xCr_yNi_{(100-x-y)}$ MPEAs (Li et al., 2021b). It has been demonstrated that this method can accurately establish the relationship between composition and ultimate tension strength. The optimum CoCrNi MPEA can be obtained (**Figure 12A**). More interestingly, some researchers tried to construct an artificial neural networks-like structure to describe the relationship between "composition-heat treatments-microstructures-properties", for revealing their potential physics mechanism (Steingrimsson et al., 2021). Another important application is to identity and/or optimize the microstructure of MPEAs. The optimal grain size of heterogeneous-grained CrCoFeNi MPEA has been determined by integrating active learning strategy, a physical model and atomic simulation (Li L. et al., 2021). The surrogate model between elemental characteristics and long-term ordering structure in MPEAs is constructed by ANN, whose prediction accuracy can be up to 87% (Zhao C. et al., 2021) (**Figure 12B**). Furthermore, the deep learning-based optimization, generation, and explanation algorithm (Lee et al., 2021) is proposed to further improve the accuracy and look for the key parameters for phase predictions. The prediction accuracy can be up to 93.1%, which far exceeds results from previous literature. In addition, the mixing entropy and mixing enthalpy are accurately identified.

In physics, machine learning is widely used to develop many-body alloy interatomic potentials for MPEAs, such as Gaussian approximation potential (Bartók et al., 2010) and spectral neighbor analysis potential (Chen et al., 2017), whose accuracy can be comparable with that from first principle calculation yet with higher efficiency. Meanwhile, the combination of machine learning potential and MD simulation has been successfully used to predict the physical properties (Dai et al., 2020), such as lattice constant, TEC, and phonon thermal conductivity in

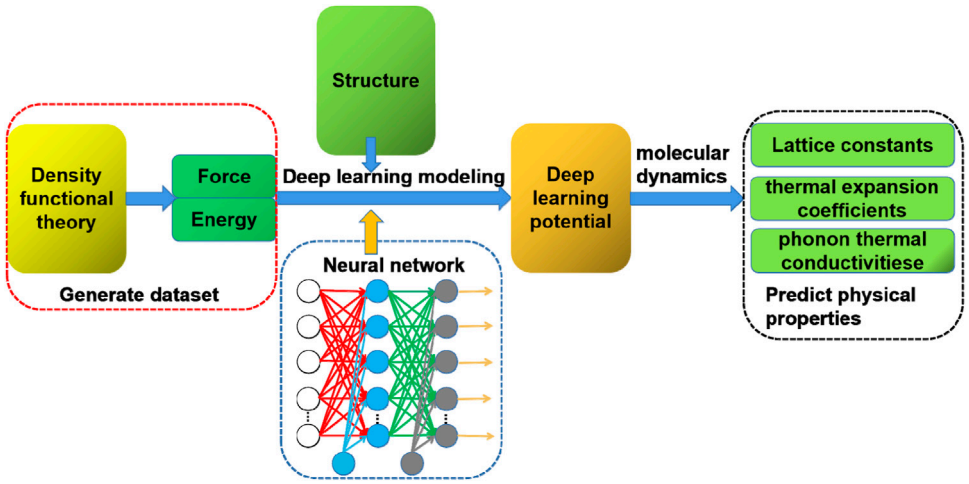

FIGURE 13 | The flowchart of the combinatorial approach for predicting the physical properties of $(Zr_{0.2}Hf_{0.2}Ti_{0.2}Nb_{0.2}Ta_{0.2})C$ MPEA.

$(Zr_{0.2}Hf_{0.2}Ti_{0.2}Nb_{0.2}Ta_{0.2})C$ MPEA (**Figure 13**). Furthermore, a combinatorial computational method is proposed to develop the new magnetic MPEAs. High-throughput method is utilized to screen out promising magnetic MPEAs, and then machine learning, additive manufacturing and CALPHAD methods are used to further predict the magnetic property (Chaudhary et al., 2021). Using DFT calculation and machine learning, *OH and *O adsorption energies on the surface of IrPdPtRhRu MPEA can be accurately predicted, which provides a useful strategy to discover the new MPEAs with outstanding catalytic activity (Batchelor et al., 2019). Moreover, this strategy is also used to predict the CO and hydrogen adsorption energies on the surface of CoCuGaNiZn and AgAuCuPdPt MPEAs, which can effectively optimize the MPEA compositions to prevent the formation of molecular hydrogen and accelerate the reduction of CO (Pedersen et al., 2020).

Future Research

The combination of machine learning and multi-scale models can quickly and accurately develop high-performance MPEAs to shorten the research-development cycle, and reduces resource costs, as well as broaden the applications of MPEA in mechanics, physics and chemistry. However, the existing multi-scale simulation methods in MPEA have not yet covered the meso-scale microstructures, such as short-range order, dislocation cell and dislocation wall, which is an important challenge in the future. Machine learning could be a feasible method to solve this problem.

MEDICINE

Biomedical metal materials are adopted to diagnose, replace, and/or repair the damaged cells, tissues, and organs by directly contacting or interacting with the human body. These kinds of special function metal materials have been widely used as medical apparatus and instruments and biological implants, such as the scalpel and artificial bone (Laing et al., 1967; Liu et al., 2004). Over the past few decades, the most widely used metal materials in medical applications are Co-based alloys, titanium alloys, stainless steel, shape-memory alloys (SMAs), and some noble metals (Vidal and Muñoz, 2009; Bertrand et al., 2010). However, many problems have arisen since these conventional biomedical alloys were used in clinical treatments, such as unsatisfactory mechanical properties or corrosion-resistant performance. For example, β-Ti alloys as the most widely employed bio-metallic materials possess lower elastic modulus than other alloys, but they exhibit lower yielding strength (Niinomi et al., 2002). Therefore, these problems extremely limit their large-scale applications in medical engineering.

Human Implants

An important application for metallic biomaterials is used as human implants, which requires the materials to have low elastic moduli. The newly developed MPEAs (González-Masís et al., 2021) possess high yielding strength/hardness and corrosion resistance as well as good blood compatibility, compared with conventional alloys. By introducing specific alloying elements, the problem about corrosion resistance and biocompatibility can be easily tackled. The most difficulty is how to effectively achieve the collaborative design between the elastic modulus and yielding strength/hardness to obtain excellent comprehensive mechanical properties. Recently, a novel TiAlFeCoNi MPEA prepared by high-pressure torsion shows an equivalent elastic modulus 170–580% higher hardness and better cellular metabolic activity 260–1,020% compared to Ti-based biomaterials (Edalati et al., 2020). Furthermore, the TiNbTaZr-based MPEAs have also been widely investigated, whose possesses superior yielding strength and better cell density compared with traditional alloys (**Figure 14**). The equal-atomic TiZrNbTaMo MPEA has compressive yield strength 1,390 MPa, plastic strain 6%, and elastic modulus 153 GPa (Wang and Xu, 2017). Moreover, the proposed $TiZrHfCr_{0.2}Mo$ and $TiZrHfCo_{0.07}Cr_{0.07}Mo$ show better biocompatibility than that of pure Ti and its alloys (Nagase et al., 2020). These excellent properties are generally due to four core effects of MPEAs, the high mixing entropy, severe lattice distortion, sluggish diffusion effect and cocktail

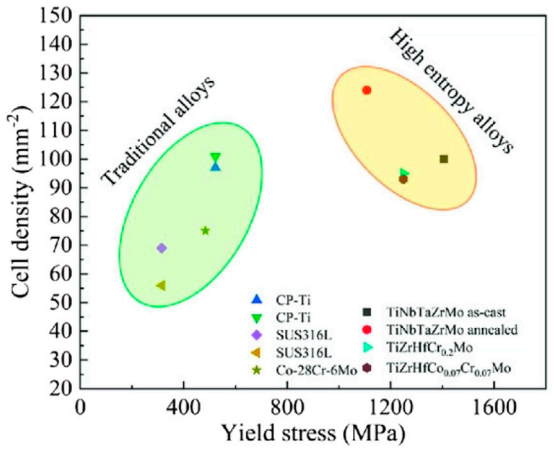

FIGURE 14 | Yield strength vs. biocompatibility in MPEAs and traditional alloys (Li et al., 2021a).

effect. For instance, severe lattice distortion not only enhances the lattice-friction stress, but also improves biocompatibility in bio-MPEAs. The cocktail effect enables the advantages of each alloy element to be brought into a full play, which allows special performance requirements to be met. Furthermore, the bio-corrosion behavior and biocompatibility of TiZrHfNbTa MPEA are investigated (Yang et al., 2020). The bio-corrosion performance can be comparable of that of Ti6Al4V alloy under biological fluids attributed to the formation of the oxide passive films on the TiZrHfNbTa surface. Meanwhile, TiZrHfNbTa MPEA provides a suitable environment for the proliferation of MC3T3-E1 pre-osteoblasts, indicating the excellent biocompatibility.

Medical Coating

Up to now, NiTi-based SMAs have been the most popular metallic materials in medical applications, such as the metal prosthesis and vascular stent. However, the release of Ni ions with significant cytotoxicity and carcinogenicity from NiTi-based SMAs during applications remains a problem to be tackled (Shabalovskaya et al., 2008; Wang et al., 2011). Conventional surface-treatment processes like physical vapor deposition or oxygen ion implantation are adopted to form a TiO_2 passive layer on the surface to prevent the Ni ion release and improve corrosion resistance. Nevertheless, a brittle TiO_2 coating is easy to form cracks under complex loads, resulting in the release of Ni ions from the broken points (Aun et al., 2016).

Recently, MPEAs have attracted a widespread attention from medicine and the related area due to their excellent mechanical properties and biocompatibility. The equimolar TiTaNbZrHf MPEA is first proposed as a medical-coating material used in NiTi-based SMAs (Motallebzadeh et al., 2018; Aksoy et al., 2019). Compared with the bare NiTi-based SMAs, the MPEA-coated NiTi-based SMAs keep the release amount of Ni ions below the safe value of 9 ppm in both the artificial saliva and gastric fluid after the 28 days static immersion. Moreover, the equimolar TiTaNbZrHf MPEA is used in the biomedical Ti6Al4V alloy as a coating material (Tüten et al., 2019). The Ti6Al4V alloy is the most commonly-used biomaterials as human implants. However, a high wear rate and the release of the cytotoxic Al and V ions limit its large-scale employment. The MPEA passive films possess a uniform surface morphology and fine-grained amorphous structure, thus improving the comprehensive mechanical properties. In addition, the enhancement of hardness induced by the MPEA passive film can significantly improve the fraction coefficient and wear resistance, thus preventing fatigue, crack, and even failure. Meanwhile, the release of Al and V ions is effectively reduced. Though the equimolar TiTaNbZrHf MPEA performs well as medical coating materials, relevant research is still in its infancy. Therefore, further exploration for other MPEA system like lightweight MPEA is needed for obtaining better performance.

Outstanding Issue

In summary, extraordinary mechanical properties are the fundamental reasons why MPEAs become widely used medical material. Moreover, future investigations are presented as follows. For example, elemental homogenization has been demonstrated to effectively improve MPEAs related biomedical properties. Therefore, how to optimize processing methods to prevent elemental segregation is crucial. In addition, existing coating approaches need to be further improved to adapt the vast composition space of MPEAs.

BIOLOGY

Antibiosis

From ancient times to the present, pathogenic-bacteria/mould-induced diseases, such as influenza, dysentery, and cholera, greatly influences the human health. Therefore, many researchers are committed into developing novel materials with high antibacterial performance. The precipitation of Cu ions in alloys can effectively destroy the protein structure in the bacteria, thus inhibiting the replication of the bacterial DNA and the synthesis of related proteins/enzymes. The release of Ag ions is easy to bind with S atoms in protein, thus effectively destroying bacterial protein structures (Chernousova and Epple, 2013; Lou et al., 2016; Yang et al., 2016). At present, a series of antibacterial stainless steels like ferritic, martensitic as well as austenitic antibacterial stainless steels are developed by introducing an appropriate amount of the Cu element because the Ag element is expensive and difficult to smelt. However, their large scale applications are limited by the insufficient broad-spectrum antibacterial and antibacterial persistence as well as the strict restrictions on the content of the Cu element for maintaining good mechanical properties and corrosion resistance (Nan et al., 2008; Ren et al., 2011).

The MPEAs can contain a high content of the Cu element, which significantly enhances the antibacterial properties of the alloy, while keeping outstanding comprehensive mechanical properties. Meanwhile, due to the huge composition space, using the cocktail effect, MPEAs can be used in various complex service conditions by introducing different elements, which greatly broadens the application range of antibacterial materials and its development prospects. Recently, a novel $Al_{0.4}$CoCrCuFeNi antibacterial high entropy alloy (AHEA)

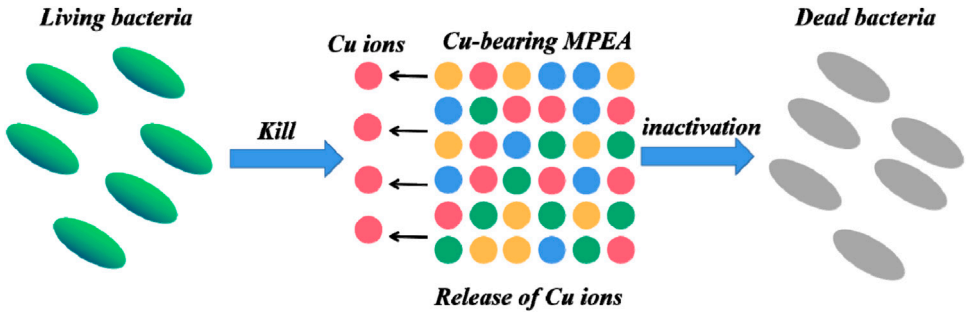

FIGURE 15 | The antibacterial mechanism of Cu-bearing MPEA.

prepared by arc-melting is proposed, whose mechanical properties and antibacterial performance thoroughly defeat conventional Cu-bearing stainless steels (Zhou et al., 2020). The results show that the antibacterial rate against common marine Gram negative *Pseudomonas aeruginosa* and Gram positive *Bifidobacterium Vietnam* can be up to 99%, attributed to a high content of the Cu element induced the release of high concentration of Cu ions from the AHEA, as shown in **Figure 15**. Meanwhile, the AHEA also possesses superior yielding strengths and corrosion resistance than traditional Cu-bearing stainless steels. Because of the abuse of antibiotics over the whole world, some bacteria exhibit high multi-drug-resistance (MDR). Lately, another CoCrCuFeNi AHEA has been successfully synthesized based on the research on the $Al_{0.4}$CoCrCuFeNi AHEA (Gao et al., 2022). The experimental results suggest that the bacteria resistance against the Gram-negative *Acinetobacter baumannii* and Gram-positive *methicillin-resistant Staphylococcus aureus* of the new CoCrCuFeNi AHEA can approach ~99%, far exceeding the conventional Cu-bearing stainless steel. Further research shows that the AHEA not only effectively removes the planktonic bacteria, but also prevents the formation of the biofilm. Moreover, compared with the as-cast CoCrCuFeNi AHEA mentioned above, the AHEA prepared using the selective laser melting and *in-situ* alloying method significantly improves the release of Cu ions, and meanwhile, possesses good mechanical properties. More importantly, the combination of the AHEA and selective laser melting method provides a feasible avenue for fabricating some medical equipment with complex shape or structures and high antibacterial performance.

Antivirus

Different from bacteria, the virus can only survive by replicating themselves in a living body. The virus usually consists of the essential genetic material (RNA or DNA) and a protein shell that wraps and protects genetic material. Since the ancient times, the existence of the virus has been always a great threat for human health due to their various spreading ways like air, surface contact and water, as well as high variability (Alhamlan et al., 2017). Although antiviral drugs can destroy the virus structure and prevent its replication, the spreading of the virus due to the direct contact on the living body cannot be effectively blocked. Therefore, the development of high performance antivirus material is extremely important and necessary.

The MPEAs containing the copper element have attracted widespread attention as the high performance antibacterial materials. In addition, Cu-bearing MPEAs have also been reported as antivirus materials. The inactivation rate against the influenza virus H1N1 and enterovirus 71 of the CuFeCoCrNi MPEA can be over 99% in the surface (Li Z. et al., 2021). It can be attributed to that aqueous corrosion induced the release of copper ions (Cu^{+} or Cu^{2+}), which can form chelate by destroying the nucleic acids and the proteins of the virus, thus leading to the inactivation of the virus. Besides, the formation of a solid metallic oxide like CuO on the surface of the Cu-bearing MPEA can also result in the denaturation of virus. Based on the design concept of MPEAs, the researchers further prepared the Al0.4CuFeCoCrNi MPEA by the addition of the Al element (Li Z. et al., 2021). The results show that the MPEA not only keeps the same antivirus performance as CuFeCoCrNi MPEA, but also possesses superior corrosion resistance and mechanical properties.

Suggested Future Work

In conclusion, because of excellent antibacterial/antivirus performance, the Cu/Ag-bearing MPEAs can be promising antibacterial/antivirus materials. Nevertheless, current related research activities are still insufficient. The optimization of the design concept and process routes for developing novel bio-MPEAs remains a great challenge to be tackled.

ENVIRONMENT

Hydrogen Storage

The CO_2 emission induced by the use of fossil fuels is mainly responsible for global greenhouse effect, which has greatly led to the global climate change. As a feasible clean energy to replace traditional fossil fuels, hydrogen has attracted widespread attention from the related fields. However, hydrogen storage remains a huge obstacle for engineering applications due to the flammability of hydrogen. The common hydrogen-storage technologies include liquefied hydrogen storage, metal-hydride hydrogen storage, and high-pressure hydrogen storage (Durbin and Malardier-Jugroot, 2013; Züttel, 2003, 2004). Among them, metallic hydride is regarded as the outstanding hydrogen-storage material because of its low cost, high volume storage density, and excellent

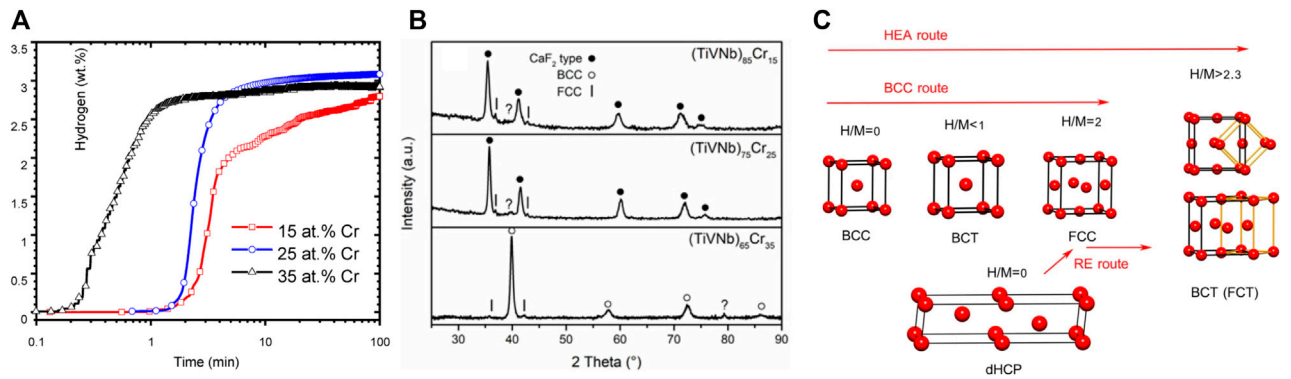

FIGURE 16 | Kinetic curves of Ti-V-Nb-Cr MPEA system under room temperature. **(A)** XRD patterns of Ti-V-Nb-Cr MPEA system after hydrogen absorption **(B)** (Strozi et al., 2021). The evolution of microstructure in TiVZrNbHf MPEA during the hydrogen-storage **(C)** (Sahlberg et al., 2016).

absorption/desorption ability (Sakintuna et al., 2007). Recently, MPEAs have been widely reported as the hydrogen-storage material.

The first proposed MPEAs for hydrogen absorption/desorption are the Co-Fe-Mn-Ti-V-Zr system (Kao et al., 2010). The $CoFeMnTi_xVZr$, $CoFeMnTiV_yZr$, and $CoFeMnTiVZr_z$ MPEAs have been demonstrated to be capable of hydrogen absorption/desorption when keeping $0.5 \leq x \leq 2.5$, $0.4 \leq y \leq 3.0$, $0.4 \leq z \leq 3.0$, respectively, via the pressure-composition isotherms (PCIs) tests and kinetic tests under an initial pressure of 9.58 atm. The hydrogen-storage performance of the alloys can be optimized by controlling elemental segregation, formation enthalpy of metal hydride, and lattice constant. In addition, high entropy effect induced the formation of single C14 Laves phase in these alloys can further improve hydrogen-storage performance. Recently, the hydrogen-storage performance of three MPEAs synthesized by arc-melting, including $(TiVNb)_{85}Cr_{15}$, $(TiVNb)_{75}Cr_{25}$ and $(TiVNb)_{65}Cr_{35}$, has been studied (Strozi et al., 2021). The three MPEAs are composed of BCC structure, and especially, they can absorb hydrogen without any activation treatment under room temperature, which can be up to H/M ~2 (**Figures 16A,B**). Furthermore, the CrFeNiTiVZr MPEA prepared by laser engineered net shaping (LENS) has also been investigated (Kunce et al., 2013). The MPEA consists of the C14 Laves phase and a little α-Ti solid-solution phase. The C14 Laves phase dominates the hydrogen storage, and the hydrogen-storage capacity of the MPEAs can be up to 1.8 wt% of H_2. The microstructure evolution in MPEAs during the hydrogen storage is also important for further improving the hydrogen-storage performance. In the recent researches, the hydrogen absorption performance of TiVZrNbHf MPEA is investigated (Sahlberg et al., 2016). The experimental results show that the novel TiVZrNbHf MPEA exhibits maximum H/M ratio of 2.5, whose capability can be comparable to that of rare-earth elements. The excellent hydrogen-storage performance of this MPEA results from the strain in the distorted FCC or BCT structure in metallic hydride, and promotes the occupation of hydrogen on tetrahedral and octahedral sites (**Figure 16C**). Furthermore, the *in situ* SR-XRD result shows that the phase transition from BCC phase to FCC dihydride phase occurs during the hydrogen-absorption process in the TiZrNbHfTa MPEA (Zlotea et al., 2019).

Decolorization

The discharge of industrial wastewater containing azo dyes is a great threat to the environment and human health (Ramirez et al., 2007; Sarlar et al., 2020). However, the degradation of azo dyes remains a huge obstacle due to the existence of a stable azo bond (-N=N-) (Tang and An, 1995). Decolorization of wastewater is an effective way to degrade azo dyes. Recently, metallic materials, such as Fe, Mg, Al, and Zn pure elements and their alloys, have been widely used to achieve the degradation of industrial wastewater due to low cost, high efficiency, and easy preparation compared with other traditional technologies (Wang P. et al., 2017; Zhang C. et al., 2017). Nevertheless, their larger scale applications are greatly limited because of poor corrosion resistance and mechanical properties. Therefore, it is urgent to develop novel alloy systems for the degradation of azo dyes.

Over the few years, due to the excellent decolorizing performance to azo dyes and outstanding mechanical properties, MPEAs have attracted widespread attention. A newly-developed AlCoCrTiZn MPEA prepared by mechanical alloying is studied (Lv et al., 2016). The results show that the novel MPEA possesses a high degradation performance to the Direct Blue 6 (a kind of azo dye), which can be comparable to the results observed in the best amorphous alloy reported to this day. The prominent performance of the MPEA to the decolorization of azo dyes can be attributed to their unique atomic structure compared with traditional alloys, consisting of higher specific surface area, unique chemical composition effects, and severer lattice distortion. These characteristics significantly reduce the activation-energy barrier (~30 kJ/mol), leading to reaction easier to occur compared to the Fe-based metallic glass (**Figure 17**). Furthermore, the AlFeMnTiM (M = Cr, Co, and Ni) MPEAs have been successfully synthesized via mechanical alloying, which have high efficiency to the decolorizing of azo dye Direct Blue 6 (Wu et al., 2019). Especially, AlFeMnTiCr shows the best decolorizing efficiency and superior catalytic performance, whose degradation performance towards azo dye far exceeds that of common commercial Fe-Si-B amorphous alloy ribbons, even 100 times better than that of industrial zero-valent iron powders. The outstanding decolorizing efficiency mainly owns to the unique atomic structure and the galvanic-cell effect.

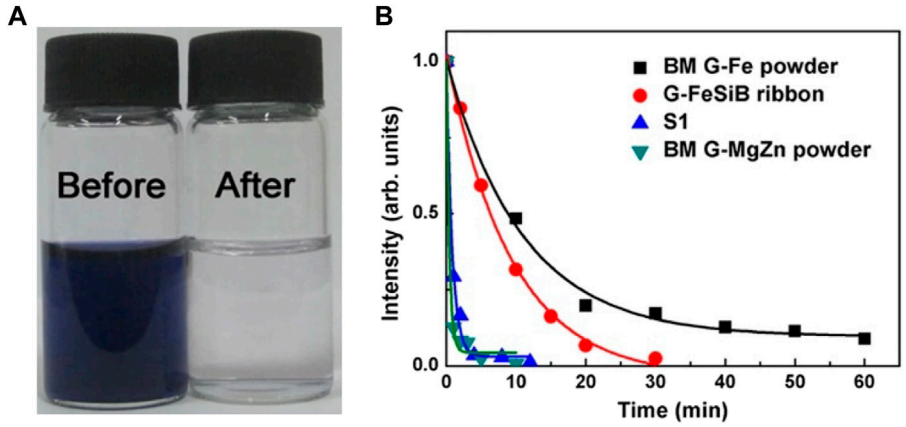

FIGURE 17 | (A) The decolorizing performance to azo dyes DB6, **(B)** the comparison of decolorizing performance with other alloys (Lv et al., 2016).

In general, MPEAs have proved to be valuable and promising decolorizing material for the degradation of the industrial wastewater.

Future Direction

In short, the outstanding hydrogen storage capacity and decolorizing performance can be attributed to the unique atomic structure, phase stability, severe lattice distortion and four core effects of MPEAs. Nevertheless, there are still some problems that limit the large-scale commercial application of MPEAs. For example, a high mass element like Hf/Zr could decrease the hydrogen-storage performance. Therefore, the lightweight elements could be introduced in the MPEAs in the future to achieve the higher hydrogen-storage ability. In addition, because of rapid reaction between azo dyes and powder MPEAs, how to effectively control the reaction rate is crucial for reducing the consumption of MPEAs and improving their recyclability.

X APPLICATIONS

In addition to these disciplines, the dynamic-development trend of MPEAs is bound to affect the following disciplines: 1) Geoscience. The exploitation and utilization of nonmetallic/metallic mines for MEAs affect geology, geomorphology, hydrogeology, mineralogy, petrology, and limnology; 2) Anthropology. The transfer of large-scale mines drives the population movement across regions and countries; 3) Economics. The rare-earth metal and noble metal used in MPEAs would undoubtedly affect the price fluctuation of the products from their compositions; 4) Psychology. The emergency of MPEAs has broken the thinking set in the traditional metallurgy strategy, which is an important breakthrough in the cognitive psychology for natural science; 5) Art. The excellent mechanical properties and unique chemical properties of MPEAs greatly broaden the selection of materials for the artwork, which could be more suitable for artists' ideas and creation; 6) Linguistics. The infinite combination space of MPEAs requires the corresponding new vocabulary to describe. The different permutations and combinations of its words gave birth to new words and promoted the development of phonology; 7) Cognitive science. The new concept and new composition system of MPEAs have expanded human beings' new understanding.

Of course, this is an important reflection from the big scientific field, to discuss the impact of the development of MPEAs on the progress of society in a wide range.

CONCLUDING REMARKS

This review describes the applications of MPEAs on engineering, including mechanics, physics, chemistry, medical science, biology, environment, computer as well as unknown areas. Based on the performance oriented material research and development mode, this approach make it easier to grasp potential application areas. Several outstanding features are summarized, which include the extreme temperature performance, irradiation performance, catalytic performance, and so on. In the future, some potential development points are also considered. This paper puts more emphasis on the application development, to promote scientific progress and technological change in multi-principal element materials.

AUTHOR CONTRIBUTIONS

JL, QF, and PL conceived the original ideas and supervised this study. YC and BX wrote original draft. BL and YC carried out the revision of this paper.

FUNDING

The authors would like to deeply appreciate the National Natural Science Foundation of China (51871092, 12072109, and 12172123), and Natural Science Foundation of Hunan Province (2021JJ40032). PL very much appreciates the supports from the National Science Foundation (DMR-1611180 and 1809640).

REFERENCES

Abareshi, M., and Emadoddin, E. (2011). Effect of Retained Austenite Characteristics on Fatigue Behavior and Tensile Properties of Transformation Induced Plasticity Steel. *Mater. Des.* 32, 5099–5105. doi:10.1016/j.matdes.2011.06.018

Aksoy, C. B., Canadinc, D., and Yagci, M. B. (2019). Assessment of Ni Ion Release from TiTaHfNbZr High Entropy alloy Coated NiTi Shape Memory Substrates in Artificial Saliva and Gastric Fluid. *Mater. Chem. Phys.* 236, 121802. doi:10.1016/j.matchemphys.2019.121802

Alhamlan, F. S., Majumder, M. S., Brownstein, J. S., Hawkins, J., Al-Abdely, H. M., Alzahrani, A., et al. (2017). Case Characteristics Among Middle East Respiratory Syndrome Coronavirus Outbreak and Non-outbreak Cases in Saudi Arabia from 2012 to 2015. *BMJ open* 7, e011865. doi:10.1136/bmjopen-2016-011865

Aun, D. P., Houmard, M., Mermoux, M., Latu-Romain, L., Joud, J.-C., Berthomé, G., et al. (2016). Development of a Flexible Nanocomposite TiO2 Film as a Protective Coating for Bioapplications of Superelastic NiTi Alloys. *Appl. Surf. Sci.* 375, 42–49. doi:10.1016/j.apsusc.2016.03.064

Bae, J. W., Seol, J. B., Moon, J., Sohn, S. S., Jang, M. J., Um, H. Y., et al. (2018). Exceptional Phase-Transformation Strengthening of Ferrous Medium-Entropy Alloys at Cryogenic Temperatures. *Acta Materialia* 161, 388–399. doi:10.1016/j.actamat.2018.09.057

Bagot, P. A. J., Kruska, K., Haley, D., Carrier, X., Marceau, E., Moody, M. P., et al. (2014). Oxidation and Surface Segregation Behavior of a Pt-Pd-Rh Alloy Catalyst. *J. Phys. Chem. C* 118, 26130–26138. doi:10.1021/jp508144z

Bartók, A. P., Payne, M. C., Kondor, R., and Csányi, G. (2010). Gaussian Approximation Potentials: The Accuracy of Quantum Mechanics, without the Electrons. *Phys. Rev. Lett.* 104, 136403. doi:10.1103/physrevlett.104.136403

Batchelor, T. A. A., Pedersen, J. K., Winther, S. H., Castelli, I. E., Jacobsen, K. W., and Rossmeisl, J. (2019). High-entropy Alloys as a Discovery Platform for Electrocatalysis. *Joule* 3, 834–845. doi:10.1016/j.joule.2018.12.015

Bertrand, E., Gloriant, T., Gordin, D. M., Vasilescu, E., Drob, P., Vasilescu, C., et al. (2010). Synthesis and Characterisation of a New Superelastic Ti-25Ta-25Nb Biomedical alloy. *J. Mech. Behav. Biomed. Mater.* 3, 559–564. doi:10.1016/j.jmbbm.2010.06.007

Chang, X., Zeng, M., Liu, K., and Fu, L. (2020). Phase Engineering of High-Entropy Alloys. *Adv. Mater.* 32, 1907226. doi:10.1002/adma.201907226

Chaudhary, V., Chaudhary, R., Banerjee, R., and Ramanujan, R. V. (2021). Accelerated and Conventional Development of Magnetic High Entropy Alloys. *Mater. Today* 49, 231–252. doi:10.1016/j.mattod.2021.03.018

Chen, C., Deng, Z., Tran, R., Tang, H., Chu, I. H., and Ong, S. P. (2017). Accurate Force Field for Molybdenum by Machine Learning Large Materials Data. *Phys. Rev. Mater.* 1, 043603. doi:10.1103/physrevmaterials.1.043603

Chen, G., Qiao, J. W., Jiao, Z. M., Zhao, D., Zhang, T. W., Ma, S. G., et al. (2019). Strength-ductility Synergy of Al0.1CoCrFeNi High-Entropy Alloys with Gradient Hierarchical Structures. *Scripta Materialia* 167, 95–100. doi:10.1016/j.scriptamat.2019.04.002

Chen, M.-R., Lin, S.-J., Yeh, J.-W., Chuang, M.-H., Chen, S.-K., and Huang, Y.-S. (2006). Effect of Vanadium Addition on the Microstructure, Hardness, and Wear Resistance of Al0.5CoCrCuFeNi High-Entropy alloy. *Metall. Mat Trans. A.* 37, 1363–1369. doi:10.1007/s11661-006-0081-3

Chen, P., Lee, C., Wang, S.-Y., Seifi, M., Lewandowski, J. J., Dahmen, K. A., et al. (2018). Fatigue Behavior of High-Entropy Alloys: A Review. *Sci. China Technol. Sci.* 61, 168–178. doi:10.1007/s11431-017-9137-4

Chen, S., Oh, H. S., Gludovatz, B., Kim, S. J., Park, E. S., Zhang, Z., et al. (2020). Real-time Observations of TRIP-Induced Ultrahigh Strain Hardening in a Dual-phase CrMnFeCoNi High-Entropy alloy. *Nat. Commun.* 11, 826–828. doi:10.1038/s41467-020-14641-1

Chen, S.-T., Tang, W.-Y., Kuo, Y.-F., Chen, S.-Y., Tsau, C.-H., Shun, T.-T., et al. (2010). Microstructure and Properties of Age-Hardenable AlxCrFe1.5MnNi0.5 Alloys. *Mater. Sci. Eng. A* 527, 5818–5825. doi:10.1016/j.msea.2010.05.052

Chernousova, S., and Epple, M. (2013). Silver as Antibacterial Agent: Ion, Nanoparticle, and Metal. *Angew. Chem. Int. Ed.* 52, 1636–1653. doi:10.1002/anie.201205923

Chou, H.-P., Chang, Y.-S., Chen, S.-K., and Yeh, J.-W. (2009). Microstructure, Thermophysical and Electrical Properties in AlxCoCrFeNi (0≤x≤2) High-Entropy Alloys. *Mater. Sci. Eng. B* 163, 184–189. doi:10.1016/j.mseb.2009.05.024

Choudhuri, D., Alam, T., Borkar, T., Gwalani, B., Mantri, A. S., Srinivasan, S. G., et al. (2015). Formation of a Huesler-like L21 Phase in a CoCrCuFeNiAlTi High-Entropy alloy. *Scripta Materialia* 100, 36–39. doi:10.1016/j.scriptamat.2014.12.006

Chuang, M.-H., Tsai, M.-H., Wang, W.-R., Lin, S.-J., and Yeh, J.-W. (2011). Microstructure and Wear Behavior of AlxCo1.5CrFeNi1.5Tiy High-Entropy Alloys. *Acta Materialia* 59, 6308–6317. doi:10.1016/j.actamat.2011.06.041

Cui, Y., Shen, J., Manladan, S. M., Geng, K., and Hu, S. (2020). Wear Resistance of FeCoCrNiMnAlx High-Entropy alloy Coatings at High Temperature. *Appl. Surf. Sci.* 512, 145736. doi:10.1016/j.apsusc.2020.145736

Cvijović, Z., and Radenković, G. (2006). Microstructure and Pitting Corrosion Resistance of Annealed Duplex Stainless Steel. *Corros Sci.* 48, 3887–3906. doi:10.1016/j.corsci.2006.04.003

Dai, F.-Z., Wen, B., Sun, Y., Xiang, H., and Zhou, Y. (2020). Theoretical Prediction on thermal and Mechanical Properties of High Entropy (Zr0.2Hf0.2Ti0.2Nb0.2Ta0.2)C by Deep Learning Potential. *J. Mater. Sci. Tech.* 43, 168–174. doi:10.1016/j.jmst.2020.01.005

Demetriou, M. D., Launey, M. E., Garrett, G., Schramm, J. P., Hofmann, D. C., Johnson, W. L., et al. (2011). A Damage-Tolerant Glass. *Nat. Mater* 10, 123–128. doi:10.1038/nmat2930

Ding, Q., Zhang, Y., Chen, X., Fu, X., Chen, D., Chen, S., et al. (2019). Tuning Element Distribution, Structure and Properties by Composition in High-Entropy Alloys. *Nature* 574, 223–227. doi:10.1038/s41586-019-1617-1

Dobeš, F., Hadraba, H., Chlup, Z., Dlouhý, A., Vilémová, M., and Matějíček, J. (2018). Compressive Creep Behavior of an Oxide-Dispersion-Strengthened CoCrFeMnNi High-Entropy alloy. *Mater. Sci. Eng. A.* 732, 99–104. doi:10.1016/j.msea.2018.06.108

Durbin, D. J., and Malardier-Jugroot, C. (2013). Review of Hydrogen Storage Techniques for on Board Vehicle Applications. *Int. J. Hydrogen Energ.* 38, 14595–14617. doi:10.1016/j.ijhydene.2013.07.058

Edalati, P., Floriano, R., Tang, Y., Mohammadi, A., Pereira, K. D., Luchessi, A. D., et al. (2020). Ultrahigh Hardness and Biocompatibility of High-Entropy alloy TiAlFeCoNi Processed by High-Pressure Torsion. *Mater. Sci. Eng. C* 112, 110908. doi:10.1016/j.msec.2020.110908

Esmaily, M., Svensson, J. E., Fajardo, S., Birbilis, N., Frankel, G. S., Virtanen, S., et al. (2017). Fundamentals and Advances in Magnesium alloy Corrosion. *Prog. Mater. Sci.* 89, 92–193. doi:10.1016/j.pmatsci.2017.04.011

Fan, Z., Wang, H., Wu, Y., Liu, X., and Lu, Z. (2017). Thermoelectric Performance of PbSnTeSe High-Entropy Alloys. *Mater. Res. Lett.* 5, 187–194. doi:10.1080/21663831.2016.1244116

Fang, Q., Chen, Y., Li, J., Jiang, C., Liu, B., Liu, Y., et al. (2019). Probing the Phase Transformation and Dislocation Evolution in Dual-phase High-Entropy Alloys. *Int. J. Plasticity* 114, 161–173. doi:10.1016/j.ijplas.2018.10.014

Fang, Q., Chen, Y., Li, J., Liu, Y., and Liu, Y. (2018). Microstructure and Mechanical Properties of FeCoCrNiNb High-Entropy alloy Coatings. *Physica B: Condensed Matter* 550, 112–116. doi:10.1016/j.physb.2018.08.044

Feng, H., Cui, S., Chen, H., Song, X., Fang, Q., Li, J., et al. (2020). A Molecular Dynamics Investigation into Deformation Mechanism of Nanotwinned Cu/high Entropy alloy FeCoCrNi Nanolaminates. *Surf. Coat. Tech.* 401, 126325. doi:10.1016/j.surfcoat.2020.126325

Feng, R., Zhang, C., Gao, M. C., Pei, Z., Zhang, F., Chen, Y., et al. (2021). High-throughput Design of High-Performance Lightweight High-Entropy Alloys. *Nat. Commun.* 12, 1–10. doi:10.1038/s41467-021-24523-9

Feng, X., Zhang, J., Xia, Z., Fu, W., Wu, K., Liu, G., et al. (2018). Stable Nanocrystalline NbMoTaW High Entropy alloy Thin Films with Excellent Mechanical and Electrical Properties. *Mater. Lett.* 210, 84–87. doi:10.1016/j.matlet.2017.08.129

Fredj, N. B., Nasr, M. B., Rhouma, A. B., Braham, C., and Sidhom, H. (2004). Fatigue Life Improvements of the AISI 304 Stainless Steel Ground Surfaces by Wire Brushing. *J. Mater. Eng. Perform.* 13, 564–574. doi:10.1361/15477020420819

Gadelmeier, C., Haas, S., Lienig, T., Manzoni, A., Feuerbacher, M., and Glatzel, U. (2020). Temperature Dependent Solid Solution Strengthening in the High Entropy alloy CrMnFeCoNi in Single Crystalline State. *Metals* 10 (11), 1412. doi:10.3390/met10111412

Gao, J., Jin, Y., Fan, Y., Xu, D., Meng, L., Wang, C., et al. (2022). Fabricating Antibacterial CoCrCuFeNi High-Entropy alloy via Selective Laser Melting and *In-Situ* Alloying. *J. Mater. Sci. Tech.* 102, 159–165. doi:10.1016/j.jmst.2021.07.002

Gao, M. C., Zhang, B., Yang, S., and Guo, S. M. (2016). Senary Refractory High-Entropy alloy HfNbTaTiVZr. *Metall. Mat Trans. A.* 47, 3333–3345. doi:10.1007/s11661-015-3105-z

Gao, X.-H., Guo, Z.-M., Geng, Q.-F., Ma, P.-J., Wang, A.-Q., and Liu, G. (2017). Enhanced Optical Properties of TiN-Based Spectrally Selective Solar Absorbers Deposited at a High Substrate Temperature. *Solar Energ. Mater. Solar Cell* 163, 91–97. doi:10.1016/j.solmat.2017.01.023

Gludovatz, B., Hohenwarter, A., Catoor, D., Chang, E. H., George, E. P., and Ritchie, R. O. (2014). A Fracture-Resistant High-Entropy alloy for Cryogenic Applications. *Science* 345, 1153–1158. doi:10.1126/science.1254581

González-Masís, J., Cubero-Sesin, J. M., Campos-Quirós, A., and Edalati, K. (2021). Synthesis of Biocompatible High-Entropy alloy TiNbZrTaHf by High-Pressure Torsion. *Mater. Sci. Eng. A.* 825, 141869. doi:10.1016/j.msea.2021.141869

Guo, H.-X., He, C.-Y., Qiu, X.-L., Shen, Y.-Q., Liu, G., and Gao, X.-H. (2020). A Novel Multilayer High Temperature Colored Solar Absorber Coating Based on High-Entropy alloy MoNbHfZrTi: Optimized Preparation and Chromaticity Investigation. *Solar Energ. Mater. Solar Cell* 209, 110444. doi:10.1016/j.solmat.2020.110444

Guo, W., Zhang, K., Liang, Z., Zou, R., and Xu, Q. (2019). Electrochemical Nitrogen Fixation and Utilization: Theories, Advanced Catalyst Materials and System Design. *Chem. Soc. Rev.* 48, 5658–5716. doi:10.1039/c9cs00159j

Gupta, R. K., and Birbilis, N. (2015). The Influence of Nanocrystalline Structure and Processing Route on Corrosion of Stainless Steel: a Review. *Corrosion Sci.* 92, 1–15. doi:10.1016/j.corsci.2014.11.041

Gwalani, B., Ayyagari, A. V., Choudhuri, D., Scharf, T., Mukherjee, S., Gibson, M., et al. (2018). Microstructure and Wear Resistance of an Intermetallic-Based Al0.25Ti0.75CoCrFeNi High Entropy alloy. *Mater. Chem. Phys.* 210, 197–206. doi:10.1016/j.matchemphys.2017.06.034

Hadraba, H., Chlup, Z., Dlouhy, A., Dobes, F., Roupcova, P., Vilemova, M., et al. (2017). Oxide Dispersion Strengthened CoCrFeNiMn High-Entropy alloy. *Mater. Sci. Eng. A* 689, 252–256. doi:10.1016/j.msea.2017.02.068

Haidemenopoulos, G. N., Kermanidis, A. T., Malliaros, C., Dickert, H. H., Kucharzyk, P., and Bleck, W. (2013). On the Effect of Austenite Stability on High Cycle Fatigue of TRIP 700 Steel. *Mater. Sci. Eng. A* 573, 7–11. doi:10.1016/j.msea.2013.02.015

Han, K., Jiang, H., Huang, T., and Wei, M. (2020). Thermoelectric Properties of CoCrFeNiNbx Eutectic High Entropy Alloys. *Crystals* 10, 762. doi:10.3390/cryst10090762

Hansson, C. M. (2011). The Impact of Corrosion on Society. *Metall. Mat Trans. A.* 42, 2952–2962. doi:10.1007/s11661-011-0703-2

He, C.-Y., Gao, X.-H., Dong, M., Qiu, X.-L., An, J.-H., Guo, H.-X., et al. (2020). Further Investigation of a Novel High Entropy alloy MoNbHfZrTi Based Solar Absorber Coating with Double Antireflective Layers. *Solar Energ. Mater. Solar Cell* 217, 110709. doi:10.1016/j.solmat.2020.110709

He, C.-Y., Gao, X.-H., Yu, D.-M., Guo, H.-X., Zhao, S.-S., and Liu, G. (2021). Highly Enhanced thermal Robustness and Photothermal Conversion Efficiency of Solar-Selective Absorbers Enabled by High-Entropy alloy Nitride MoTaTiCrN Nanofilms. *ACS Appl. Mater. Inter.* 13 (14), 16987–16996. doi:10.1021/acsami.0c23011

He, J. Y., Liu, W. H., Wang, H., Wu, Y., Liu, X. J., Nieh, T. G., et al. (2014). Effects of Al Addition on Structural Evolution and Tensile Properties of the FeCoNiCrMn High-Entropy alloy System. *Acta Materialia* 62, 105–113. doi:10.1016/j.actamat.2013.09.037

Hemphill, M. A., Yuan, T., Wang, G. Y., Yeh, J. W., Tsai, C. W., Chuang, A., et al. (2012). Fatigue Behavior of Al0.5CoCrCuFeNi High Entropy Alloys. *Acta Materialia* 60, 5723–5734. doi:10.1016/j.actamat.2012.06.046

Hou, J., Zhang, M., Yang, H., Qiao, J., and Wu, Y. (2019). Surface Strengthening in Al0.25CoCrFeNi High-Entropy alloy by Boronizing. *Mater. Lett.* 238, 258–260. doi:10.1016/j.matlet.2018.12.029

Hsu, C.-Y., Sheu, T.-S., Yeh, J.-W., and Chen, S.-K. (2010). Effect of Iron Content on Wear Behavior of AlCoCrFexMo0.5Ni High-Entropy Alloys. *Wear* 268, 653–659. doi:10.1016/j.wear.2009.10.013

Huang, E., Clausen, B., Wang, Y., Choo, H., Liaw, P., Benson, M., et al. (2007). A Neutron-Diffraction Study of the Low-Cycle Fatigue Behavior of HASTELLOY C-22HSTM alloy. *Int. J. Fatigue* 29, 1812–1819. doi:10.1016/j.ijfatigue.2007.01.025

Huang, K., Wang, G., Qing, H., Chen, Y., and Guo, H. (2021a). Effect of Cu Content on Electrical Resistivity, Mechanical Properties and Corrosion Resistance of AlCuxNiTiZr0.75 High Entropy alloy Films. *Vacuum* 195, 110695. doi:10.1016/j.vacuum.2021.110695

Huang, L., Wang, X., Zhao, X., Wang, C., and Yang, Y. (2021b). Analysis on the Key Role in Corrosion Behavior of CoCrNiAlTi-Based High Entropy alloy. *Mater. Chem. Phys.* 259, 124007. doi:10.1016/j.matchemphys.2020.124007

Huo, W., Fang, F., Liu, X., Tan, S., Xie, Z., and Jiang, J. (2019). Fatigue Resistance of Nanotwinned High-Entropy alloy Films. *Mater. Sci. Eng. A* 739, 26–30. doi:10.1016/j.msea.2018.09.112

Huo, W., Liu, X., Tan, S., Fang, F., Xie, Z., Shang, J., et al. (2018). Ultrahigh Hardness and High Electrical Resistivity in Nano-Twinned, Nanocrystalline High-Entropy alloy Films. *Appl. Surf. Sci.* 439, 222–225. doi:10.1016/j.apsusc.2018.01.050

Islam, M. A., Chen, S., and Tomota, Y. (2007). Tensile and Plane Bending Fatigue Properties of Two TRIP Steels at Room Temperature in the Air-A Comparative Study. *J. Materi Eng. Perform.* 16, 248–253. doi:10.1007/s11665-007-9045-z

Jin, G., Cai, Z., Guan, Y., Cui, X., Liu, Z., Li, Y., et al. (2018a). High Temperature Wear Performance of Laser-Cladded FeNiCoAlCu High-Entropy alloy Coating. *Appl. Surf. Sci.* 445, 113–122. doi:10.1016/j.apsusc.2018.03.135

Jin, X., Zhou, Y., Zhang, L., Du, X., and Li, B. (2018b). A Novel Fe 20 Co 20 Ni 41 Al 19 Eutectic High Entropy alloy with Excellent Tensile Properties. *Mater. Lett.* 216, 144–146. doi:10.1016/j.matlet.2018.01.017

Joseph, J., Haghdadi, N., Annasamy, M., Kada, S., Hodgson, P. D., Barnett, M. R., et al. (2020). On the Enhanced Wear Resistance of CoCrFeMnNi High Entropy alloy at Intermediate Temperature. *Scripta Materialia* 186, 230–235. doi:10.1016/j.scriptamat.2020.05.053

Joseph, J., Hodgson, P., Jarvis, T., Wu, X., Stanford, N., and Fabijanic, D. M. (2018). Effect of Hot Isostatic Pressing on the Microstructure and Mechanical Properties of Additive Manufactured AlxCoCrFeNi High Entropy Alloys. *Mater. Sci. Eng. A* 733, 59–70. doi:10.1016/j.msea.2018.07.036

Kang, Y. B., Shim, S. H., Lee, K. H., and Hong, S. I. (2018). Dislocation Creep Behavior of CoCrFeMnNi High Entropy alloy at Intermediate Temperatures. *Mater. Res. Lett.* 6, 689–695. doi:10.1080/21663831.2018.1543731

Kao, Y.-F., Chen, S.-K., Chen, T.-J., Chu, P.-C., Yeh, J.-W., and Lin, S.-J. (2011). Electrical, Magnetic, and Hall Properties of AlxCoCrFeNi High-Entropy Alloys. *J. Alloys Compd.* 509, 1607–1614. doi:10.1016/j.jallcom.2010.10.210

Kao, Y.-F., Chen, S.-K., Sheu, J.-H., Lin, J.-T., Lin, W.-E., Yeh, J.-W., et al. (2010). Hydrogen Storage Properties of Multi-Principal-Component CoFeMnTixVyZrz Alloys. *Int. J. Hydrogen Energ.* 35, 9046–9059. doi:10.1016/j.ijhydene.2010.06.012

Kim, D. G., Jo, Y. H., Yang, J., Choi, W.-M., Kim, H. S., Lee, B.-J., et al. (2019). Ultrastrong Duplex High-Entropy alloy with 2 GPa Cryogenic Strength Enabled by an Accelerated Martensitic Transformation. *Scripta Materialia* 171, 67–72. doi:10.1016/j.scriptamat.2019.06.026

Körmann, F., Ikeda, Y., Grabowski, B., and Sluiter, M. H. F. (2017). Phonon Broadening in High Entropy Alloys. *NPJ Comput. Mater.* 3, 1–9. doi:10.1038/s41524-017-0037-8

Koyama, M., Zhang, Z., Wang, M., Ponge, D., Raabe, D., Tsuzaki, K., et al. (2017). Bone-like Crack Resistance in Hierarchical Metastable Nanolaminate Steels. *Science* 355, 1055–1057. doi:10.1126/science.aal2766

Kral, P., Blum, W., Dvorak, J., Yurchenko, N., Stepanov, N., Zherebtsov, S., et al. (2020). Creep Behavior of an AlTiVNbZr0.25 High Entropy alloy at 1073 K. *Mater. Sci. Eng. A* 783, 139291. doi:10.1016/j.msea.2020.139291

Kunce, I., Polanski, M., and Bystrzycki, J. (2013). Structure and Hydrogen Storage Properties of a High Entropy ZrTiVCrFeNi alloy Synthesized Using Laser Engineered Net Shaping (LENS). *Int. J. Hydrogen Energ.* 38, 12180–12189. doi:10.1016/j.ijhydene.2013.05.071

Laing, P. G., Ferguson, A. B., Jr, and Hodge, E. S. (1967). Tissue Reaction in Rabbit Muscle Exposed to Metallic Implants. *J. Biomed. Mater. Res.* 1, 135–149. doi:10.1002/jbm.820010113

Lee, C. W., Yang, K. D., Nam, D.-H., Jang, J. H., Cho, N. H., Im, S. W., et al. (2018). Defining a Materials Database for the Design of Copper Binary alloy Catalysts for Electrochemical CO2 Conversion. *Adv. Mater.* 30, 1704717. doi:10.1002/adma.201704717

Lee, S. Y., Byeon, S., Kim, H. S., Jin, H., and Lee, S. (2021). Deep Learning-Based Phase Prediction of High-Entropy Alloys: Optimization, Generation, and Explanation. *Mater. Des.* 197, 109260. doi:10.1016/j.matdes.2020.109260

Lei, Z., Liu, X., Wu, Y., Wang, H., Jiang, S., Wang, S., et al. (2018). Enhanced Strength and Ductility in a High-Entropy alloy via Ordered Oxygen Complexes. *Nature* 563, 546–550. doi:10.1038/s41586-018-0685-y

Li, J., Chen, H., Fang, Q., Jiang, C., Liu, Y., and Liaw, P. K. (2020a). Unraveling the Dislocation-Precipitate Interactions in High-Entropy Alloys. *Int. J. Plasticity* 133, 102819. doi:10.1016/j.ijplas.2020.102819

Li, J., Chen, H., He, Q., Fang, Q., Liu, B., Jiang, C., et al. (2020c). Unveiling the Atomic-Scale Origins of High Damage Tolerance of Single-crystal High Entropy Alloys. *Phys. Rev. Mater.* 4, 103612. doi:10.1103/physrevmaterials.4.103612

Li, J., Fang, Q., and Liaw, P. K. (2021a). Microstructures and Properties of High-Entropy Materials: Modeling, Simulation, and Experiments. *Adv. Eng. Mater.* 23, 2001044. doi:10.1002/adem.202001044

Li, J. L., Li, Z., Wang, Q., Dong, C., and Liaw, P. K. (2020b). Phase-field Simulation of Coherent BCC/B2 Microstructures in High Entropy Alloys. *Acta Materialia* 197, 10–19. doi:10.1016/j.actamat.2020.07.030

Li, J., Xie, B., Fang, Q., Liu, B., Liu, Y., and Liaw, P. K. (2021b). High-throughput Simulation Combined Machine Learning Search for Optimum Elemental Composition in Medium Entropy alloy. *J. Mater. Sci. Tech.* 68, 70–75. doi:10.1016/j.jmst.2020.08.008

Li, L., Xie, B., Fang, Q., and Li, J. (2021c). Machine Learning Approach to Design High Entropy Alloys with Heterogeneous Grain Structures. *Metall. Mater. Trans. A.* 52, 439–448. doi:10.1007/s11661-020-06099-z

Li, P., Wang, A., and Liu, C. T. (2017b). A Ductile High Entropy alloy with Attractive Magnetic Properties. *J. Alloys Compd.* 694, 55–60. doi:10.1016/j.jallcom.2016.09.186

Li, P., Wang, A., and Liu, C. T. (2017a). Composition Dependence of Structure, Physical and Mechanical Properties of FeCoNi(MnAl) X High Entropy Alloys. *Intermetallics* 87, 21–26. doi:10.1016/j.intermet.2017.04.007

Li, Q., Xue, S., Wang, J., Shao, S., Kwong, A. H., Giwa, A., et al. (2018). High-Strength Nanotwinned Al Alloys with 9R Phase. *Adv. Mater.* 30, 1704629. doi:10.1002/adma.201704629

Li, Z., Gu, Y., Pan, M., Wang, C., Wu, Z., Hou, X., et al. (2019). Tailoring AC Magnetic Properties of FeCoNi(MnSi) ($0 \le X \le 0.4$) High-Entropy Alloys by the Addition of Mn and Si Elements. *J. Alloys Compd.* 792, 215–221. doi:10.1016/j.jallcom.2019.03.411

Li, Z., Pradeep, K. G., Deng, Y., Raabe, D., and Tasan, C. C. (2016). Metastable High-Entropy Dual-phase Alloys Overcome the Strength-Ductility Trade-Off. *Nature* 534, 227–230. doi:10.1038/nature17981

Li, Z., Qiao, D., Xu, Y., Zhou, E., Yang, C., Yuan, X., et al. (2021d). Cu-bearing High-Entropy Alloys with Excellent Antiviral Properties. *J. Mater. Sci. Tech.* 84, 59–64. doi:10.1016/j.jmst.2020.12.027

Liang, H., Yao, H., Qiao, D., Nie, S., Lu, Y., Deng, D., et al. (2019). Microstructures and Wear Resistance of AlCrFeNi2W0.2Nbx High-Entropy alloy Coatings Prepared by Laser Cladding. *J. Therm. Spray Tech.* 28, 1318–1329. doi:10.1007/s11666-019-00901-0

Liu, C. M., Wang, H. M., Zhang, S. Q., Tang, H. B., and Zhang, A. L. (2014). Microstructure and Oxidation Behavior of New Refractory High Entropy Alloys. *J. Alloys Compd.* 583, 162–169. doi:10.1016/j.jallcom.2013.08.102

Liu, H., Liu, J., Li, X., Chen, P., Yang, H., and Hao, J. (2020). Effect of Heat Treatment on Phase Stability and Wear Behavior of Laser Clad AlCoCrFeNiTi0.8 High-Entropy alloy Coatings. *Surf. Coat. Tech.* 392, 125758. doi:10.1016/j.surfcoat.2020.125758

Liu, J., Liu, H., Chen, P., and Hao, J. (2019). Microstructural Characterization and Corrosion Behaviour of AlCoCrFeNiTix High-Entropy alloy Coatings Fabricated by Laser Cladding. *Surf. Coat. Tech.* 361, 63–74. doi:10.1016/j.surfcoat.2019.01.044

Liu, K., Nene, S. S., Frank, M., Sinha, S., and Mishra, R. S. (2019). Extremely High Fatigue Resistance in an Ultrafine Grained High Entropy alloy. *Appl. Mater. Today* 15, 525–530. doi:10.1016/j.apmt.2019.04.001

Liu, K., Nene, S. S., Frank, M., Sinha, S., and Mishra, R. S. (2018). Metastability-assisted Fatigue Behavior in a Friction Stir Processed Dual-phase High Entropy alloy. *Mater. Res. Lett.* 6, 613–619. doi:10.1080/21663831.2018.1523240

Liu, L., Zhang, Y., Han, J., Wang, X., Jiang, W., Liu, C. T., et al. (2021). Nanoprecipitate-strengthened High-entropy Alloys. *Adv. Sci.* 8, 2100870. doi:10.1002/advs.202100870

Liu, X., Chu, P., and Ding, C. (2004). Surface Modification of Titanium, Titanium Alloys, and Related Materials for Biomedical Applications. *Mater. Sci. Eng. R: Rep.* 47, 49–121. doi:10.1016/j.mser.2004.11.001

Liu, X. T., Lei, W. B., Ma, L. J., Liu, J. L., Liu, J., and Cui, J. Z. (2016). Effect of boron on the Microstructure, Phase Assemblage and Wear Properties of Al0.5CoCrCuFeNi High-Entropy alloy. *Rare Metal Mat Eng.* 45, 2201–2207. doi:10.1016/s1875-5372(17)30003-6

Löbel, M., Lindner, T., Mehner, T., and Lampke, T. (2018). Influence of Titanium on Microstructure, Phase Formation and Wear Behaviour of AlCoCrFeNiTix High-Entropy alloy. *Entropy (Basel)* 20, 505. doi:10.3390/e20070505

Lou, Y., Lin, L., Xu, D., Zhao, S., Yang, C., Liu, J., et al. (2016). Antibacterial Ability of a Novel Cu-Bearing 2205 Duplex Stainless Steel against *Pseudomonas aeruginosa* Biofilm in Artificial Seawater. *Int. Biodeterioration Biodegradation* 110, 199–205. doi:10.1016/j.ibiod.2016.03.026

Lu, C.-L., Lu, S.-Y., Yeh, J.-W., and Hsu, W.-K. (2013). Thermal Expansion and Enhanced Heat Transfer in High-Entropy Alloys. *J. Appl. Cryst.* 46, 736–739. doi:10.1107/s0021889813005785

Lv, Z. Y., Liu, X. J., Jia, B., Wang, H., Wu, Y., and Lu, Z. P. (2016). Development of a Novel High-Entropy alloy with Eminent Efficiency of Degrading Azo Dye Solutions. *Sci. Rep.* 6, 34213. doi:10.1038/srep34213

Ly, A. L., and Findley, K. O. (2016). The Effects of Pre-straining Conditions on Fatigue Behavior of a Multiphase TRIP Steel. *Int. J. Fatigue* 87, 225–234. doi:10.1016/j.ijfatigue.2016.02.004

Ma, Y., Feng, Y. H., Debela, T. T., Peng, G. J., and Zhang, T. H. (2016). Nanoindentation Study on the Creep Characteristics of High-Entropy alloy Films: Fcc versus Bcc Structures. *Int. J. Refractory Met. Hard Mater.* 54, 395–400. doi:10.1016/j.ijrmhm.2015.08.010

Marshal, A., Pradeep, K. G., Music, D., Wang, L., Petracic, O., and Schneider, J. M. (2019). Combinatorial Evaluation of Phase Formation and Magnetic Properties of FeMnCoCrAl High Entropy alloy Thin Film Library. *Sci. Rep.* 9, 7864–7874. doi:10.1038/s41598-019-44351-8

Miracle, D. B., and Senkov, O. N. (2017). A Critical Review of High Entropy Alloys and Related Concepts. *Acta Materialia* 122, 448–511. doi:10.1016/j.actamat.2016.08.081

Motallebzadeh, A., Yagci, M. B., Bedir, E., Aksoy, C. B., and Canadinc, D. (2018). Mechanical Properties of TiTaHfNbZr High-Entropy alloy Coatings Deposited on NiTi Shape Memory alloy Substrates. *Metall. Mat Trans. A.* 49, 1992–1997. doi:10.1007/s11661-018-4605-4

Nagase, T., Iijima, Y., Matsugaki, A., Ameyama, K., and Nakano, T. (2020). Design and Fabrication of Ti-Zr-Hf-Cr-Mo and Ti-Zr-Hf-Co-Cr-Mo High-Entropy Alloys as Metallic Biomaterials. *Mater. Sci. Eng. C* 107, 110322. doi:10.1016/j.msec.2019.110322

Nan, L., Liu, Y., Lü, M., and Yang, K. (2008). Study on Antibacterial Mechanism of Copper-Bearing Austenitic Antibacterial Stainless Steel by Atomic Force Microscopy. *J. Mater. Sci. Mater. Med.* 19, 3057–3062. doi:10.1007/s10856-008-3444-z

Niinomi, M., Hattori, T., Morikawa, K., Kasuga, T., Suzuki, A., Fukui, H., et al. (2002). Development of Low Rigidity β-type Titanium alloy for Biomedical Applications. *Mater. Trans.* 43, 2970–2977. doi:10.2320/matertrans.43.2970

Nilsson, J. O., and Wilson, A. (1993). Influence of Isothermal Phase Transformations on Toughness and Pitting Corrosion of Super Duplex Stainless Steel SAF 2507. *Mater. Sci. Tech.* 9, 545–554. doi:10.1179/mst.1993.9.7.545

Niu, C., Zaddach, A. J., Oni, A. A., Sang, X., Hurt, J. W., Iii, LeBeau, J. M., et al. (2015). Spin-driven Ordering of Cr in the Equiatomic High Entropy alloy NiFeCrCo. *Appl. Phys. Lett.* 106, 161906. doi:10.1063/1.4918996

Pedersen, J. K., Batchelor, T. A. A., Bagger, A., and Rossmeisl, J. (2020). High-entropy Alloys as Catalysts for the CO2 and CO Reduction Reactions. *ACS Catal.* 10, 2169–2176. doi:10.1021/acscatal.9b04343

Peng, J., Li, L., Li, F., Liu, B., Zherebtsov, S., Fang, Q., et al. (2021). The Predicted Rate-dependent Deformation Behaviour and Multistage Strain Hardening in a Model Heterostructured Body-Centered Cubic High Entropy alloy. *Int. J. Plasticity* 145, 103073. doi:10.1016/j.ijplas.2021.103073

Picak, S., Wegener, T., Sajadifar, S. V., Sobrero, C., Richter, J., Kim, H., et al. (2021). On the Low-Cycle Fatigue Response of CoCrNiFeMn High Entropy alloy with

Ultra-fine Grain Structure. *Acta Materialia* 205, 116540. doi:10.1016/j.actamat.2020.116540

Poulia, A., Georgatis, E., Lekatou, A., and Karantzalis, A. E. (2016). Microstructure and Wear Behavior of a Refractory High Entropy alloy. *Int. J. Refractory Met. Hard Mater.* 57, 50–63. doi:10.1016/j.ijrmhm.2016.02.006

Qiu, X.-W., Zhang, Y.-P., He, L., and Liu, C.-g. (2013). Microstructure and Corrosion Resistance of AlCrFeCuCo High Entropy alloy. *J. Alloys Compd.* 549, 195–199. doi:10.1016/j.jallcom.2012.09.091

Qiu, X. W., Zhang, Y. P., and Liu, C. G. (2014). Effect of Ti Content on Structure and Properties of Al2CrFeNiCoCuTix High-Entropy alloy Coatings. *J. Alloys Compd.* 585, 282–286. doi:10.1016/j.jallcom.2013.09.083

Rahul, M. R., Samal, S., Venugopal, S., and Phanikumar, G. (2018). Experimental and Finite Element Simulation Studies on Hot Deformation Behaviour of AlCoCrFeNi2.1 Eutectic High Entropy alloy. *J. Alloys Compd.* 749, 1115–1127. doi:10.1016/j.jallcom.2018.03.262

Ramirez, J. H., Maldonado-Hódar, F. J., Pérez-Cadenas, A. F., Moreno-Castilla, C., Costa, C. A., and Madeira, L. M. (2007). Azo-dye Orange II Degradation by Heterogeneous Fenton-like Reaction Using Carbon-Fe Catalysts. *Appl. Catal. B: Environ.* 75, 312–323. doi:10.1016/j.apcatb.2007.05.003

Ranganathan, S. (2003). Alloyed Pleasures: Multimetallic Cocktails. *Cur Sci.* 85, 1404–1406.

Reddy, N. S., Krishnaiah, J., Young, H. B., and Lee, J. S. (2015). Design of Medium Carbon Steels by Computational Intelligence Techniques. *Comput. Mater. Sci.* 101, 120–126. doi:10.1016/j.commatsci.2015.01.031

Ren, L., Nan, L., and Yang, K. (2011). Study of Copper Precipitation Behavior in a Cu-Bearing Austenitic Antibacterial Stainless Steel. *Mater. Des.* 32, 2374–2379. doi:10.1016/j.matdes.2010.11.030

Ren, S., Li, L., Fang, Q., and Li, J. (2021). Modeling and Analysis of Yielding and Strain Hardening in Metastable High-Entropy Alloys. *Phys. Status Solidi B* 258, 2100247. doi:10.1002/pssb.202100247

Rupp, M., Tkatchenko, A., Müller, K. R., and Von Lilienfeld, O. A. (2012). Fast and Accurate Modeling of Molecular Atomization Energies with Machine Learning. *Phys. Rev. Lett.* 108, 058301. doi:10.1103/PhysRevLett.108.058301

Sagar, B., Biswas, K., and Mukherjee, R. (2021). A Phase-Field Study on a Eutectic High-Entropy alloy during Solidification. *Philos. Mag. Lett.* 101, 160–172. doi:10.1080/09500839.2021.1877366

Sahlberg, M., Karlsson, D., Zlotea, C., and Jansson, U. (2016). Superior Hydrogen Storage in High Entropy Alloys. *Sci. Rep.* 6, 36770–36776. doi:10.1038/srep36770

Sakintuna, B., Lamaridarkrim, F., and Hirscher, M. (2007). Metal Hydride Materials for Solid Hydrogen Storage: A Review☆. *Int. J. Hydrogen Energ.* 32, 1121–1140. doi:10.1016/j.ijhydene.2006.11.022

Sarlar, K., Tekgül, A., and Kucuk, I. (2020). Magnetocaloric Properties in a FeNiGaMnSi High Entropy alloy. *Curr. Appl. Phys.* 20, 18–22. doi:10.1016/j.cap.2019.09.019

Schmidhuber, J. (2015). Deep Learning in Neural Networks: An Overview. *Neural Networks* 61, 85–117. doi:10.1016/j.neunet.2014.09.003

Selvakumar, N., and Barshilia, H. C. (2012). Review of Physical Vapor Deposited (PVD) Spectrally Selective Coatings for Mid- and High-Temperature Solar thermal Applications. *Solar Energ. Mater. Solar Cell* 98, 1–23. doi:10.1016/j.solmat.2011.10.028

Senkov, O. N., Scott, J. M., Senkova, S. V., Miracle, D. B., and Woodward, C. F. (2011a). Microstructure and Room Temperature Properties of a High-Entropy TaNbHfZrTi alloy. *J. Alloys Compd.* 509, 6043–6048. doi:10.1016/j.jallcom.2011.02.171

Senkov, O. N., and Semiatin, S. L. (2015). Microstructure and Properties of a Refractory High-Entropy alloy after Cold Working. *J. Alloys Compd.* 649, 1110–1123. doi:10.1016/j.jallcom.2015.07.209

Senkov, O. N., Wilks, G. B., Scott, J. M., and Miracle, D. B. (2011b). Mechanical Properties of Nb25Mo25Ta25W25 and V20Nb20Mo20Ta20W20 Refractory High Entropy Alloys. *Intermetallics* 19, 698–706. doi:10.1016/j.intermet.2011.01.004

Seol, J. B., Bae, J. W., Kim, J. G., Sung, H., Li, Z., Lee, H. H., et al. (2020). Short-range Order Strengthening in boron-doped High-Entropy Alloys for Cryogenic Applications. *Acta Materialia* 194, 366–377. doi:10.1016/j.actamat.2020.04.052

Shabalovskaya, S., Anderegg, J., and Van Humbeeck, J. (2008). Critical Overview of Nitinol Surfaces and Their Modifications for Medical Applications. *Acta Biomater.* 4, 447–467. doi:10.1016/j.actbio.2008.01.013

Shackelford, J. F., and Alexander, W. (2000). *CRC Materials Science and Engineering Handbook*. Boca Raton, FL: CRC Press.

Shafeie, S., Guo, S., Hu, Q., Fahlquist, H., Erhart, P., and Palmqvist, A. (2015). High-entropy Alloys as High-Temperature Thermoelectric Materials. *J. Appl. Phys.* 118, 184905. doi:10.1063/1.4935489

Shi, Y., Yang, B., and Liaw, P. (2017). Corrosion-resistant High-Entropy Alloys: A Review. *Metals* 7, 43. doi:10.3390/met7020043

Song, G., and Atrens, A. (2003). Understanding Magnesium Corrosion-A Framework for Improved Alloy Performance. *Adv. Eng. Mater.* 5, 837–858. doi:10.1002/adem.200310405

Song, H., Tian, F., Hu, Q.-M., Vitos, L., Wang, Y., Shen, J., et al. (2017). Local Lattice Distortion in High-Entropy Alloys. *Phys. Rev. Mater.* 1, 023404. doi:10.1103/physrevmaterials.1.023404

Steingrimsson, B., Fan, X., Yang, X., Gao, M. C., Zhang, Y., and Liaw, P. K. (2021). Predicting Temperature-dependent Ultimate Strengths of Body-Centered-Cubic (BCC) High-Entropy Alloys. *Npj Comput. Mater.* 7, 1–10. doi:10.1038/s41524-021-00623-4

Strozi, R. B., Leiva, D. R., Zepon, G., Botta, W. J., and Huot, J. (2021). Effects of the Chromium Content in (TiVNb)100−xCrx Body-Centered Cubic High Entropy Alloys Designed for Hydrogen Storage Applications. *Energies* 14, 3068. doi:10.3390/en14113068

Sugimouto, K.-I., Kobayashi, M., and Yasuki, S.-I. (1997). Cyclic Deformation Behavior of a Transformation-Induced Plasticity-Aided Dual-phase Steel. *Metall. Mat Trans. A.* 28, 2637–2644. doi:10.1007/s11661-997-0020-y

Sun, B., Lu, W., Gault, B., Ding, R., Makineni, S. K., Wan, D., et al. (2021a). Chemical Heterogeneity Enhances Hydrogen Resistance in High-Strength Steels. *Nat. Mater.* 20, 1629–1634. doi:10.1038/s41563-021-01050-y

Sun, L., and Cava, R. J. (2019). High-entropy alloy Superconductors: Status, Opportunities, and Challenges. *Phys. Rev. Mater.* 3, 090301. doi:10.1103/physrevmaterials.3.090301

Sun, X., Du, L., Lan, H., Cui, J., Wang, L., Li, R., et al. (2021b). Mechanical, Corrosion and Magnetic Behavior of a CoFeMn1.2NiGa0.8 High Entropy alloy. *J. Mater. Sci. Tech.* 73, 139–144. doi:10.1016/j.jmst.2020.08.062

Suresh, S. (1998). *Fatigue of Materials*. Cambridge University Press.

Tan, X. (2014). Catalyst Alloys Processing. *JOM* 66, 2176–2185. doi:10.1007/s11837-014-0984-1

Tang, W. Z., and Huren An, H. (1995). UV/TiO2 Photocatalytic Oxidation of Commercial Dyes in Aqueous Solutions. *Chemosphere* 31, 4157–4170. doi:10.1016/0045-6535(95)80015-d

Tang, Z., Yuan, T., Tsai, C.-W., Yeh, J.-W., Lundin, C. D., and Liaw, P. K. (2015). Fatigue Behavior of a Wrought Al0.5CoCrCuFeNi Two-phase High-Entropy alloy. *Acta Materialia* 99, 247–258. doi:10.1016/j.actamat.2015.07.004

Tian, Y. Z., Sun, S. J., Lin, H. R., and Zhang, Z. F. (2019). Fatigue Behavior of CoCrFeMnNi High-Entropy alloy under Fully Reversed Cyclic Deformation. *J. Mater. Sci. Tech.* 35, 334–340. doi:10.1016/j.jmst.2018.09.068

Tong, C.-J., Chen, M.-R., Yeh, J.-W., Lin, S.-J., Chen, S.-K., Shun, T.-T., et al. (2005). Mechanical Performance of the Al X CoCrCuFeNi High-Entropy alloy System with Multiprincipal Elements. *Metall. Mat Trans. A.* 36, 1263–1271. doi:10.1007/s11661-005-0218-9

Tsai, K.-Y., Tsai, M.-H., and Yeh, J.-W. (2013). Sluggish Diffusion in Co-cr-fe-mn-ni High-Entropy Alloys. *Acta Materialia* 61, 4887–4897. doi:10.1016/j.actamat.2013.04.058

Tsai, M.-H. (2013). Physical Properties of High Entropy Alloys. *Entropy* 15, 5338–5345. doi:10.3390/e15125338

Tsai, M.-H., and Yeh, J.-W. (2014). High-entropy Alloys: a Critical Review. *Mater. Res. Lett.* 2, 107–123. doi:10.1080/21663831.2014.912690

Tsai, M. T., Huang, J. C., Lin, P. H., Liu, T. Y., Liao, Y. C., Jang, J. S. C., et al. (2018). Creep of Face-Centered-Cubic {111} and {100} Grains in FeCoNiCrMn and FeCoNiCrMn Al Alloys: Orientation and Solid Solution Effects. *Intermetallics* 103, 88–96. doi:10.1016/j.intermet.2018.10.006

Tüten, N., Canadinc, D., Motallebzadeh, A., and Bal, B. (2019). Microstructure and Tribological Properties of TiTaHfNbZr High Entropy alloy Coatings Deposited on Ti6Al4V Substrates. *Intermetallics* 105, 99–106. doi:10.1016/j.intermet.2018.11.015

Vidal, C. V., and Muñoz, A. I. (2009). Effect of thermal Treatment and Applied Potential on the Electrochemical Behaviour of CoCrMo Biomedical alloy. *Electrochimica Acta* 54, 1798–1809. doi:10.1016/j.electacta.2008.10.018

Wang, A.-L., Wan, H.-C., Xu, H., Tong, Y.-X., and Li, G.-R. (2014). Quinary PdNiCoCuFe alloy Nanotube Arrays as Efficient Electrocatalysts for Methanol Oxidation. *Electrochimica Acta* 127, 448–453. doi:10.1016/j.electacta.2014.02.076

Wang, C., Fu, H., Jiang, L., Xue, D., and Xie, J. (2019a). A Property-Oriented Design Strategy for High Performance Copper Alloys via Machine Learning. *NPJ Comput. Mater.* 5, 1–8. doi:10.1038/s41524-019-0227-7

Wang, D., Liu, L., Huang, W., and Zhuang, H. L. (2019b). Semiconducting SiGeSn High-Entropy alloy: A Density Functional Theory Study. *J. Appl. Phys.* 126, 225703. doi:10.1063/1.5135324

Wang, D., Tan, J., Li, C. J., Qin, X. M., and Guo, S. F. (2021a). Enhanced Creep Resistance of Ti30Al25Zr25Nb20 High-Entropy alloy at Room Temperature. *J. Alloys Compd.* 885, 161038. doi:10.1016/j.jallcom.2021.161038

Wang, H. R., Liu, F., Zhang, Y. P., Yu, D. Z., and Wang, F. P. (2011). Preparation and Properties of Titanium Oxide Film on NiTi alloy by Micro-arc Oxidation. *Appl. Surf. Sci.* 257, 5576–5580. doi:10.1016/j.apsusc.2011.01.047

Wang, M., Ma, Z., Xu, Z., and Cheng, X. (2019c). Microstructures and Mechanical Properties of HfNbTaTiZrW and HfNbTaTiZrMoW Refractory High-Entropy Alloys. *J. Alloys Compd.* 803, 778–785. doi:10.1016/j.jallcom.2019.06.138

Wang, P., Wang, J., Huo, J., Xu, W., Wang, X., and Wang, G. (2017a). Fast Degradation of Azo Dye by Nanocrystallized Fe-Based Alloys. *Sci. China Phys. Mech.* 60, 076112. doi:10.1007/s11433-017-9034-5

Wang, S.-P., and Xu, J. (2017). TiZrNbTaMo High-Entropy alloy Designed for Orthopedic Implants: As-Cast Microstructure and Mechanical Properties. *Mater. Sci. Eng. C* 73, 80–89. doi:10.1016/j.msec.2016.12.057

Wang, X., Gao, J., Hu, H., Zhang, H., Liang, L., Javaid, K., et al. (2017b). High-temperature Tolerance in WTi-Al 2 O 3 Cermet-Based Solar Selective Absorbing Coatings with Low thermal Emissivity. *Nano Energy* 37, 232–241. doi:10.1016/j.nanoen.2017.05.036

Wang, X., Yao, H., Zhang, Z., Li, X., Chen, C., Yin, L., et al. (2021b). Enhanced Thermoelectric Performance in High Entropy Alloys Sn0.25Pb0.25Mn0.25Ge0.25Te. *ACS Appl. Mater. Inter.* 13, 18638–18647. doi:10.1021/acsami.1c00221

Wang, Y., Yang, Y., Yang, H., Zhang, M., Ma, S., and Qiao, J. (2018). Microstructure and Wear Properties of Nitrided AlCoCrFeNi High-Entropy alloy. *Mater. Chem. Phys.* 210, 233–239. doi:10.1016/j.matchemphys.2017.05.029

Wang, Z., Wang, C., Zhao, Y.-L., Hsu, Y.-C., Li, C.-L., Kai, J.-J., et al. (2020). High Hardness and Fatigue Resistance of CoCrFeMnNi High Entropy alloy Films with Ultrahigh-Density Nanotwins. *Int. J. Plasticity* 131, 102726. doi:10.1016/j.ijplas.2020.102726

Wen, C., Zhang, Y., Wang, C., Xue, D., Bai, Y., Antonov, S., et al. (2019). Machine Learning Assisted Design of High Entropy Alloys with Desired Property. *Acta Materialia* 170, 109–117. doi:10.1016/j.actamat.2019.03.010

Wu, J.-M., Lin, S.-J., Yeh, J.-W., Chen, S.-K., Huang, Y.-S., and Chen, H.-C. (2006). Adhesive Wear Behavior of AlxCoCrCuFeNi High-Entropy Alloys as a Function of Aluminum Content. *Wear* 261, 513–519. doi:10.1016/j.wear.2005.12.008

Wu, S.-k., Pan, Y., Wang, N., Lu, T., and Dai, W.-j. (2019). Azo Dye Degradation Behavior of AlFeMnTiM (M = Cr, Co, Ni) High-Entropy Alloys. *Int. J. Miner Metall. Mater.* 26, 124–132. doi:10.1007/s12613-019-1716-x

Wu, Y., Wang, C., Sun, Y., Ning, Y., Liu, Y., Xue, Y., et al. (2015). Study on the thermal Stability of Al/NbTiSiN/NbTiSiON/SiO2 Solar Selective Absorbing Coating. *Solar Energy* 119, 18–28. doi:10.1016/j.solener.2015.06.021

Wu, Z., Bei, H., Pharr, G. M., and George, E. P. (2014). Temperature Dependence of the Mechanical Properties of Equiatomic Solid Solution Alloys with Face-Centered Cubic crystal Structures. *Acta Materialia* 81, 428–441. doi:10.1016/j.actamat.2014.08.026

Xiang, C., Jiazhen, W., Huameng, F. U., En-Hou, H. A. N., Zhang, H., Jianqiu, W., et al. (2016). Corrosion Behavior of Several High-Entropy Alloys in High Temperature High Pressure Water. *J. Chin. Soc. Corro Prot.* 36, 107–112.

Xie, P., Yao, Y., Huang, Z., Liu, Z., Zhang, J., Li, T., et al. (2019). Highly Efficient Decomposition of Ammonia Using High-Entropy alloy Catalysts. *Nat. Commun.* 10, 4011–4012. doi:10.1038/s41467-019-11848-9

Yadav, S., Sarkar, S., Aggarwal, A., Kumar, A., and Biswas, K. (2018). Wear and Mechanical Properties of Novel (CuCrFeTiZn)100-xPbx High Entropy alloy Composite via Mechanical Alloying and Spark Plasma Sintering. *Wear* 410-411, 93–109. doi:10.1016/j.wear.2018.05.023

Yang, S.-M., Chen, Y.-C., Pan, Y.-T., and Lin, D.-Y. (2016). Effect of Silver on Microstructure and Antibacterial Property of 2205 Duplex Stainless Steel. *Mater. Sci. Eng. C* 63, 376–383. doi:10.1016/j.msec.2016.03.014

Yang, W., Liu, Y., Pang, S., Liaw, P. K., and Zhang, T. (2020). Bio-corrosion Behavior and *In Vitro* Biocompatibility of Equimolar TiZrHfNbTa High-Entropy alloy. *Intermetallics* 124, 106845. doi:10.1016/j.intermet.2020.106845

Yao, Y., Huang, Z., Xie, P., Lacey, S. D., Jacob, R. J., Xie, H., et al. (2018). Carbothermal Shock Synthesis of High-Entropy-alloy Nanoparticles. *Science* 359, 1489–1494. doi:10.1126/science.aan5412

Ye, Y. F., Wang, Q., Lu, J., Liu, C. T., and Yang, Y. (2016). High-entropy alloy: Challenges and Prospects. *Mater. Today* 19, 349–362. doi:10.1016/j.mattod.2015.11.026

Ye, Y. X., Liu, C. Z., Wang, H., and Nieh, T. G. (2018). Friction and Wear Behavior of a Single-phase Equiatomic TiZrHfNb High-Entropy alloy Studied Using a Nanoscratch Technique. *Acta Materialia* 147, 78–89. doi:10.1016/j.actamat.2018.01.014

Yeh, J.-W., Chen, S.-K., Lin, S.-J., Gan, J.-Y., Chin, T.-S., Shun, T.-T., et al. (2004). Nanostructured High-Entropy Alloys with Multiple Principal Elements: Novel Alloy Design Concepts and Outcomes. *Adv. Eng. Mater.* 6, 299–303. doi:10.1002/adem.200300567

Yin, B., and Curtin, W. A. (2019). First-principles-based Prediction of Yield Strength in the RhIrPdPtNiCu High-Entropy alloy. *NPJ Comput. Mater.* 5, 1–7. doi:10.1038/s41524-019-0151-x

Yu, D.-M., He, C.-Y., Zhao, S.-S., Guo, H.-X., Liu, G., and Gao, X.-H. (2021b). A Novel Multilayer High Temperature Solar Absorber Coating Based on High-Entropy alloy NbMoTaW: Optical Properties, thermal Stability and Corrosion Properties. *J. Materiomics* 7, 895–903. doi:10.1016/j.jmat.2021.04.006

Yu, D. M., He, C. Y., Qiu, X. L., Zhao, S. S., Guo, H. X., Liu, G., et al. (2021a). A Multilayer Solar Absorber Coating Based on NbMoTaW Refractory High Entropy alloy: Optical Properties, thermal Stability and Failure Mechanism. *Mater. Today Energ.* 21, 100789. doi:10.1016/j.mtener.2021.100789

Yu, Y., Liu, W. M., Zhang, T. B., Li, J. S., Wang, J., Kou, H. C., et al. (2014). Microstructure and Tribological Properties of AlCoCrFeNiTi0.5 High-Entropy Alloy in Hydrogen Peroxide Solution. *Metall. Mat Trans. A.* 45, 201–207. doi:10.1007/s11661-013-1982-6

Yu, Y., Wang, J., Li, J., Kou, H., Duan, H., Li, J., et al. (2015). Tribological Behavior of AlCoCrCuFeNi and AlCoCrFeNiTi0.5 High Entropy Alloys under Hydrogen Peroxide Solution against Different Counterparts. *Tribology Int.* 92, 203–210. doi:10.1016/j.triboint.2015.06.013

Zhang, C., Zhang, F., Diao, H., Gao, M. C., Tang, Z., Poplawsky, J. D., et al. (2016a). Understanding Phase Stability of Al-Co-Cr-Fe-Ni High Entropy Alloys. *Mater. Des.* 109, 425–433. doi:10.1016/j.matdes.2016.07.073

Zhang, C., Zhu, Z., and Zhang, H. (2017a). Mg-based Amorphous Alloys for Decolorization of Azo Dyes. *Results Phys.* 7, 2054–2056. doi:10.1016/j.rinp.2017.06.031

Zhang, G., Ming, K., Kang, J., Huang, Q., Zhang, Z., Zheng, X., et al. (2018a). High Entropy alloy as a Highly Active and Stable Electrocatalyst for Hydrogen Evolution Reaction. *Electrochimica Acta* 279, 19–23. doi:10.1016/j.electacta.2018.05.035

Zhang, H., Xu, W., Xu, Y., Lu, Z., and Li, D. (2018b). The thermal-mechanical Behavior of WTaMoNb High-Entropy alloy via Selective Laser Melting (SLM): experiment and Simulation. *Int. J. Adv. Manuf Technol.* 96, 461–474. doi:10.1007/s00170-017-1331-9

Zhang, M., George, E. P., and Gibeling, J. C. (2021a). Tensile Creep Properties of a CrMnFeCoNi High-Entropy alloy. *Scr Mater.* 194, 113633. doi:10.1016/j.scriptamat.2020.113633

Zhang, Q., Xu, H., Tan, X. H., Hou, X. L., Wu, S. W., Tan, G. S., et al. (2017b). The Effects of Phase Constitution on Magnetic and Mechanical Properties of FeCoNi(CuAl) (X = 0-1.2) High-Entropy Alloys. *J. Alloys Compd.* 693, 1061–1067. doi:10.1016/j.jallcom.2016.09.271

Zhang, S., Wu, C. L., Zhang, C. H., Guan, M., and Tan, J. Z. (2016b). Laser Surface Alloying of FeCoCrAlNi High-Entropy alloy on 304 Stainless Steel to Enhance Corrosion and Cavitation Erosion Resistance. *Opt. Laser Tech.* 84, 23–31. doi:10.1016/j.optlastec.2016.04.011

Zhang, X. K., Chou, T. H., Li, W. P., Wang, Y. N., Huang, J. C., and Cheng, L. (2021b). Microstructure and Mechanical Properties of (FeCoNi)100−x(NiAl)x Eutectic Multi-Principal Element Alloys. *J. Alloys Compd.* 862, 158349. doi:10.1016/j.jallcom.2020.158349

Zhang, Y., Zuo, T., Cheng, Y., and Liaw, P. K. (2013). High-entropy Alloys with High Saturation Magnetization, Electrical Resistivity, and Malleability. *Sci. Rep.* 3, 1455–1457. doi:10.1038/srep01455

Zhang, Y. M., Yang, S., and Evans, J. R. G. (2008). Revisiting Hume-Rothery's Rules with Artificial Neural Networks. *Acta Materialia* 56, 1094–1105. doi:10.1016/j.actamat.2007.10.059

Zhang, Y., Zuo, T. T., Tang, Z., Gao, M. C., Dahmen, K. A., Liaw, P. K., et al. (2014). Microstructures and Properties of High-Entropy Alloys. *Prog. Mater. Sci.* 61, 1–93. doi:10.1016/j.pmatsci.2013.10.001

Zhao, C., Li, J., Liu, Y., Wang, W. Y., Kou, H., Beaugnon, E., et al. (2021a). Tailoring Mechanical and Magnetic Properties of AlCoCrFeNi High-Entropy alloy via Phase Transformation. *J. Mater. Sci. Tech.* 73, 83–90. doi:10.1016/j.jmst.2020.08.063

Zhao, D. Q., Pan, S. P., Zhang, Y., Liaw, P. K., and Qiao, J. W. (2021b). Structure Prediction in High-Entropy Alloys with Machine Learning. *Appl. Phys. Lett.* 118, 231904. doi:10.1063/5.0051307

Zhou, E., Qiao, D., Yang, Y., Xu, D., Lu, Y., Wang, J., et al. (2020). A Novel Cu-Bearing High-Entropy alloy with Significant Antibacterial Behavior against Corrosive marine Biofilms. *J. Mater. Sci. Tech.* 46, 201–210. doi:10.1016/j.jmst.2020.01.039

Zlotea, C., Sow, M. A., Ek, G., Couzinié, J.-P., Perrière, L., Guillot, I., et al. (2019). Hydrogen Sorption in TiZrNbHfTa High Entropy alloy. *J. Alloys Compd.* 775, 667–674. doi:10.1016/j.jallcom.2018.10.108

Zou, Y., Maiti, S., Steurer, W., and Spolenak, R. (2014). Size-dependent Plasticity in an Nb25Mo25Ta25W25 Refractory High-Entropy alloy. *Acta Materialia* 65, 85–97. doi:10.1016/j.actamat.2013.11.049

Züttel, A. (2004). Hydrogen Storage Methods. *Naturwissenschaften* 91, 157–172. doi:10.1007/s00114-004-0516-x

Züttel, A. (2003). Materials for Hydrogen Storage. *Mater. Today* 6, 24–33. doi:10.1016/S1369-7021(03)00922-2

Conflict of Interest: The authors declare that the research was conducted in the absence of any commercial or financial relationships that could be construed as a potential conflict of interest.

Publisher's Note: All claims expressed in this article are solely those of the authors and do not necessarily represent those of their affiliated organizations, or those of the publisher, the editors and the reviewers. Any product that may be evaluated in this article, or claim that may be made by its manufacturer, is not guaranteed or endorsed by the publisher.